UNIVERSITAT DE LES ILLES BALEARS

DEPARTAMENT DE FISICA

Nonlinear Dynamics of Mutually Coupled Semiconductor Lasers

Memoria de investigación presentada por Raúl Vicente Zafra, en el Departamento de Física de la UIB, Noviembre 2004.

Esta memoria de investigación ha sido dirigida por el Doctor *Claudio R. Mirasso* del Departamento de Física de la UIB.

Electronic version is available at
http://www.imedea.uib.es/PhysDept/publications/

Contents

List of Figures

Chapter 1

Introduction

IN May of 1960 Theodore H. Maiman succeeded for the very first time in History to maintain a laser action in a ruby crystal[1]. Since that milestone, the investigation and use of the laser, both in fundamental and applied Physics, has grown spectacularly. With 11 Nobel Prize winners who studied its most fundamental properties or applications, and thousands of patents related to its use in our daily life, the laser continues today revolutionizing industries such as communications or medicine.

In the brief history of the laser it stands out the almost simultaneous announcement at the end of 1962 by groups from MIT, IBM, and General Research Laboratories, the creation of the first semiconductor lasers. Its invention opened a door to the miniaturization, cheapness, and consequently massive use of this type of devices in multitude of applications we use in our everyday life. This kind of lasers, besides of having very interesting properties for practical applications, shows a huge gain coefficient and an inherent non-linearity that make them excellent candidates to develop dynamical instabilities of high interest for academics and industry.

At the beginning of the laser era, to achieve a stable power, highly colimated, and spectrally pure laser beam, at the same time that avoiding any type of instability was the dream of any experimental researcher in laser applications. However, it took little time to realize that the laser constituted a non-linear dynamical system able to generate a rich variety of behaviors and that we could take advantage of it. Hence, in the present the understanding and control of the different dynamical instabilities affecting a given type of lasers form an important field of research, which includes methods and techniques from dynamical systems theory to quantum optics. The generation of ultra-short pulses, all-optical processing of information, creation of carrier signals in the microwave range, or cryptography based on chaotic communications, are just a few examples of applications that benefitted from our present control on the dynamics of lasers.

---

[1]Interestingly several investigators though to have demonstrated that by that time laser emission could not be generated with ruby as amplifier medium.

In this memoire we try to contribute to the study of the instabilities that arise when a semiconductor laser is subject to a given type of perturbation. Thus, the application of a modulation to the current supply of the laser, an injection of light in its active region, or the insertion of a feedback loop, represent a few examples of external perturbations that are able to considerably affect the behavior and characteristics of the laser. In special, in the forthcoming chapters the dynamical consequences of bidirectionally couple two semiconductor lasers are studied. In this configuration of mutually coupled lasers, the behavior of each laser depends on the state of the other through a given interaction. In our case the coupling is optoelectronic, i.e., part of the light emitted by each laser is detected and the photocurrent generated is added to the bias current of the other laser. Both the absolute and relative dynamics between the lasers, and the synchronization phenomenon will be evaluated in this system. In spite of the fact that the results here presented have been exclusively predicted for the coupling of semiconductor lasers, most of the phenomena we investigate seem to be independent of the particular characteristics of this type of laser and therefore they are expected to occur in more general models of coupled oscillators with time delay. In fact, not only semiconductor lasers but neurons, chemical oscillators, or Josephson junctions are just a few examples of non-linear systems, whose connection or coupling with similar units may lead to a very rich dynamics.

While the dynamics of coupled oscillators have been extensively studied, only recently have the effects of finite connection time, which naturally arise from the finite propagation speed of the signals between the subsystems, been taken into account. In our case, the time it takes the light emitted from a laser to reach the photodetector plus the time it takes the transmission of the generated photocurrent to the other laser constitutes our interaction delay time between the lasers. The inclusion of these delay times in a given model not only introduces an infinite dimensional phase space[1] but also provides a new source of possible instabilities. In this direction and due to its possible consequences in physics, medicine, biology, and chemistry, an special attention has been recently captured by the phenomenon denominated "Death by delay"[2, 3, 4, 5, 6] by which oscillation death of two coupled limit cycle oscillators is induced through the delayed interaction between them. A new observation of this phenomenon, with no counterpart for instantaneously coupled identical oscillators, is reported in the Results chapter.

In the forthcoming chapters we include the following material. In this chapter we continue by presenting some basic concepts and tools used along this investigation. These contains the stability analysis for fixed points in a system of delay differential equations, some types of bifurcations and the most relevant definitions associated to the phenomena of synchronization. Chapter II, after introducing and modeling the system under study, collects the main results of this research. These are focused on the properties of synchronization between the lasers. The modification of the Arnold tongues (or

regions where both lasers pulse at the same frequency) with the delay between lasers and the prediction of localized synchronization in our system as a consequence of a spontaneous symmetry breaking are subjected to analysis. Moreover, we predict and experimentally found the "death by delay" effect in our semiconductor laser setup. We show that when the lasers are subjected to a delay feedback loop, the condition that a delay in needed in the coupling line in order to observe the quenching phenomena is waived. Experimental data confirming several theoretical predictions are also presented at the end of the chapter. Finally, in the chapter devoted to concluding the memoire, we summarize and highlight the most important results as well as we plot some possible lines of continuing the work presented here.

1.1 Once upon a laser

Stimulated emission is the process by which light passing through a fluorescent material can be amplified. The proposal of this mechanism in the light-matter interaction by Albert Einstein in 1916 is usually considered the beginning of the laser theoretical foundation. Einstein introduced the concept of induced or stimulated emission when studying the thermal equilibrium of a set of atoms with the electromagnetic radiation. He noticed that besides the absorption and spontaneous emission of a photon by an atomic system, a new process was necessary in order to recover from thermodynamical arguments the Planck formula for the black body radiation. Thus, the concept by which the encountering of an excited atom with a photon, which is resonant with an atomic transition, causes the emission of an identical photon, was first devised.

Although the first experimental evidence of stimulated emission was observed by Ladenburg and Kopferman in 1928, the interest on this effect decreased among the physicists. The main reason was the apparent impossibility of creating inverted populations with more atoms in the excited state than the ground state so that absorption would not dominate the process and stimulated emission could occur. In fact, it was clear that the Boltzmannian distribution of occupation of energy levels assured that population inversion could not occur in a system in thermodynamical equilibrium. An external pumping of energy or the isolation of excited atoms could solve this problem but it was necessary to wait until 1954 so that Charles H. Townes introduced the key element for the light amplification development. His idea of placing the amplifying medium inside a resonant cavity so that an oscillation could start, provided that the gain of the stimulated emission could overcome the cavity losses, would led to the first practical microwave amplification by stimulated emission of radiation or maser[2].

---

[2]Townes and the USSR physicists Basov and Prokhorov shared the Nobel Prize in Physics in 1964 for developing the maser.

The transition from the maser to the laser, or equivalently, from the microwave to the optical domain was far from being trivial. In a seminal paper published in Physical Review in December of 1958, Townes and his postdoctoral assistant Arthur L. Schawlow described the first detailed proposal for building a laser with the fundamental idea of a pair of mirrors facing each other playing the role of the resonant cavity. The effect of the mirrors was to select from the non-directional light of the fluorescent material only those photons propagating along the cavity axis, and consequently made them to pass through the amplifying medium several times by bouncing them back and forth between the mirrors before they scape through a partially transparent mirror, and hence generating an useful laser beam. The much smaller wavelength of the visible light compared to the microwave and the problem of finding the appropriate excitation media made the experimental development of the laser an exciting and difficult one. But in May of 1960, the American physicist Theodore H. Maiman eventually achieved the first laser action[3] in a pink ruby rod with its ends silvered placed in a spring-shaped flashlamp.

Later on, many different laser systems have been successfully built but almost all of them (including the semiconductor laser that will be discussed below) still consist of the same three ingredients than the first laser, namely, a) **an active medium hosting the stimulated emission**, b) **a pumping source responsible of creating the necessary population inversion and**, c) **a cavity providing a feedback and frequency selection mechanism**.

1.2 Semiconductor lasers

1.2.1 Introduction

John Von Newmann, one of the fathers of the quantum theory, was also the first in proposing semiconductor materials as candidates to host light amplification as early as 1953. The idea of recombinating electron-hole pairs in a p-n junction was culminated when the lasing action in semiconductors was first reported in 1962 by four independent groups from MIT, IBM and General Research Laboratories. The characteristics of this type of laser considerably differed from the first laser developed only two years before and required of an extraordinary effort. The pumping mechanism consisted in electronic injection rather than the intense discharge of photons from a flashlamp as used in the ruby laser. The discrete levels of energy between which the laser transition took place in the ruby had nothing to do with the energy bands of the semiconductor materials. The laser cavity is also very special and exclusive in a semiconductor laser and it is formed by the polished facets perpendicular

---

[3]The emission of this first laser was pulsating because of the three level nature of the ruby system was unable to maintain a permanent population inversion.

to the junction plane through the reflectivity that provides the index change in the interface of the semiconductor material and the air.

In 1963 Kroemer in USA and Alferov and Kazarinov in USSR independently suggested the crucial improvement of the heterostructure semiconductor laser. The heterostructure consists of placing the active material sandwiched between two semiconductor layers with a wider band gap. The huge injection current reduction necessary to operate these new lasers and the improvement of characteristics such as the optical confinement were improved so much by the heterostructure addition that with the advent of the first practical demonstration of this type of lasers in 1969, the semiconductor laser became for the very first time the small, cheap and fast source of light widely used today.

Of course, a lot of advances have taken place since those early days of the semiconductor laser history, but here we only want to mention the breakthrough supposed the introduction of the vertical cavity surface emitting lasers (VCSEL's) in 1979. From the design point of view, the main novelty this laser introduced was the fact that the output of light was normal to the junction plane, instead of parallel as in the conventional edge-emitter lasers. Nowadays, this type of lasers are a hot topic of research and they offer a much better performance for most of applications where a cheap, low power, and compact source of light is needed. However, they suffer the problem of an uncontrolled dynamics of the polarization of the light they emit. The study of the mutual coupling of VCSEL's is currently under investigation by the author, as it is mentioned in the Conclusions chapter, as an extension of the work on bidirectional setups presented here.

1.2.2   Semiconductor laser rate equations

Most of lasers are typically described through three macroscopic variables consisting of the electric field, population inversion, and material polarization. Depending on the time scales in which the three variables decay, none of them, one, or even two of these variables can be adiabatically eliminated. A classification of lasers is made according to the number of variables eliminated. Hence, Class C lasers are those in which the three decay constants are of the same order of magnitude and no adiabatic elimination of any of the variables proceeds. In this case the three variables are needed to accurately describe the main physical processes in the laser. In Class B lasers only one of the variables is eliminated and two of them are still required to capture the dynamics of the laser. Finally, in Class A lasers, only one variable governs the evolution of the system. Since in a semiconductor the relaxation time for the polarization is much shorter than for the rest of variables, it can be adiabatically eliminated and the semiconductor laser falls into the Class B group. Due to the complex nature of the electric field ($E = \sqrt{S}e^{i\varphi}$, where S is the optical intensity and φ is the optical phase) we end up with three equations,

which can be deduced from Maxwell and Schrödinger equations after a series of important approximations, describing the semiconductor laser

$$\frac{dS}{dt} = (\Gamma rmg - \gamma_c)S \tag{1.1}$$

$$\frac{dN}{dt} = \frac{J}{ed} - \gamma_s N - \mathrm{g}S \tag{1.2}$$

$$\frac{d\varphi}{dt} = \frac{1}{2}\alpha(\Gamma\mathrm{g} - \gamma_\mathrm{c}), \tag{1.3}$$

where the N stands for the population inversion, γ_c is the photon decay rate, γ_s is the carrier decay rate, J is the current density injection, and $g = g(N, S)$ is the gain function.

As we can see, for a solitary laser the optical phase is just an slave of the population inversion and optical intensity variables, and as a consequence the dynamics of the these variables are decoupled from the phase. This means that a semiconductor laser cannot exhibit chaotic dynamics because at least three ordinary differential equations are required in order to observe that complex behavior, and only two equations are coupled in the system of Eqs. (1.1)-(1.3). However, the effect of external perturbations on the semiconductor laser introduces additional degrees of freedom able to excite very rich complex dynamical states as bistability, excitability, or chaos. Among the diversity of ways of perturbing a laser, we point out the injection of light into the active region of the laser, the feedback of light from the same laser into its own active region, and the modulation of the current supply ($J = J(t)$). Any of these modifications of the solitary laser setup is subject to a great deal of analysis by the researchers because of intrinsic and applications interests. **In this work we study another kind of perturbation that consists of the mutual coupling of two semiconductor lasers and that allow us to study the phenomenon of synchronization**, which is introduced in the next section.

1.3   Synchronization

Once two oscillating objects (in our case semiconductor lasers) are connected or coupled through any kind of weak interaction, these systems are usually capable of adjusting of their rhythms of oscillation, or in other words to synchronize. The fundamentals of this synchronization phenomena, which we will study in forthcoming chapters for semiconductor lasers, were first noticed by the great Dutch scientist Christiaan Huygens as early as 1665. While staying at bed for a couple of days watching two clocks hanging on a common support, Huygens observed "a wonderful effect that nobody could have thought before" and which later on in his memoirs he described as

... It is quite worth noting that when we suspended two clocks so constructed from two hooks embedded in the same wooden beam, the motions of each pendulum in opposite swings were so much in agreement that they never receded the least bit from each other and the sound of each was always heard simultaneously.

1.3.1 Definition

The modern concept of synchronization is an **adjustment of rhythms of oscillating objects due to their weak interaction**. According to this definition two objects are susceptible to synchronize when isolated they are able to oscillate by themselves, i.e., they are self-sustained oscillators. It is important to make clear that the resonance phenomena of forced systems that have no rhythm on their own are not synchronization processes. Moreover, it is necessary to stress that the interaction should be weak enough so that qualitatively each oscillator does not change its uncoupled dynamics. Otherwise, a too strong coupling between subsystems can be understood as we are dealing with a new unified system where each subsytem has not its own identity. It is also important to note that the coupling between different oscillatory units can be asymmetric. This is, the coupling strength may be not identical in the two directions of the interaction. The extreme case is the unidirectional coupling, where a system (master) influences another system (slave) but the reverse is not true. In the general case, both units perturb the state of the other and it is said that there is a mutual or bidirectional coupling.

In the following, the more important phenomena associated to the synchronization concept are introduced as well as some basic definitions.

1.3.2 Frequency locking

The main hallmark of synchronization is the so-called frequency locking. When uncoupled two oscillators use to exhibit a certain mistmach in their natural frequencies or detuning $\Delta\nu_o = \nu_{o2} - \nu_{o1}$. That is, the signal of each system oscillates with a different frequency. However, once coupled if the detuning is small enough both systems can oscillate at exactly the same frequency for a finite range of detuning. This entrainment of frequencies to a common value $\nu_{f1} = \nu_{f2} = \nu_f$ is known as frequency locking. The difference in the natural frequencies or detuning susceptible to experience the locking phenomena is dependent of the interaction strength κ_c between the oscillators. The region in the κ_c versus $\Delta\nu_o$ plane where such a locking occurs is usually called synchronization area or **Arnold tongue**. If the detuning parameter is very large, higher order synchronization regions may appear where the ratio between frequencies after coupling occurs is a rational number, i.e., $\nu_{f1}/\nu_{f2} = q/p \in \mathbb{Q}$. We speak then of synchronization of order p : q.

1.3.3   Phase locking

Besides the amplitude of a signal its phase is also a fundamental source of information. The phase is used to parameterize the limit cycle (attractor in the phase space of the oscillatory system) on which the dynamics is taking place, so that it grows monotonically and increase a value of 2π each full oscillation. When the difference between the phases of two oscillators is bounded we say they are phase locked. More generally, we can consider phase locking of order **p** : **q** if $|p\phi_1 - q\phi_2| <$ constant. Usually, when $|\phi_1 - \phi_2| = 0$ it is said that the oscillators exhibit in-phase dynamics, and when $|\phi_1 - \phi_2| = \pi$ it is named anti-phase dynamics, as in the original observation of Huygens with the pendula swinging in opposition.

A generalization of the concept of phase $\phi(t)$ for an arbitrary signal $x(t)$ can be introduced via the construction of the complex analytical signal $x(t) + iy(t) = A(t)\exp^{i\phi(t)}$, where $y(t)$ is the Hilbert transform of $x(t)$

$$y(t) = \frac{1}{\pi} P.V. \int_{-\infty}^{\infty} \frac{x(t')}{t-t'}dt',$$

and P.V. stands for Cauchy principal value. Consequently, the same definitions of phase synchronization are valid for this generalized phase and they can be applied now for non-periodic or even chaotic signals.

1.3.4   Different kinds of synchronization

Several types of synchronization have been reported in the literature depending on the relationship that the signals $x_1(t)$, and $x_2(t)$ of two interacting systems may exhibit.

The simplest case occurs when two coupled systems generate an identical output, $x_1(t) = x_2(t)$. Far from trivial, it was noticed that this phenomena could be observed even in chaotic systems and receives the name of **identical or complete synchronization**. This identical solution is just a form of a more general type of synchronization called **generalized**, where a given function $\mathbb{F}$ relates the two outputs $x_1(t) = \mathbb{F}(x_2(t))$. When $\mathbb{F}$ is the identity the identical synchronization is recovered. **Localized synchronization** stands for the case in which both systems oscillate at common frequency but with very different amplitudes. The term **phase synchronization** is usually referred to the case in which the phase difference between the two outputs is bounded but their amplitudes stay uncorrelated. Another type of synchronization that shows up in different setups is the **lag synchronization**. This solution, which usually appears as an intermediate stage between the phase and complete synchronization, is very common in subsystems interacting with a time delay. The lag solution or synchronization stands for the equality of the two output signals once one of them has been appropriately shifted in time, i.e., $x_1(t) = x_2(t-\tau)$. Of course, some of the previous definitions can be adapted

to more general cases as arrays of oscillators with a number of units larger than two or even oscillatory media.

The degree of quality of most types of synchronizations (identical, localized, and lag) is usually measured by computing indicators such as the cross-correlation function

$$\Gamma(\tau) = \frac{\sum_i \left[(x_1(i) - \overline{x}_1)(x_2(i - \tau) - \overline{x}_2)\right]}{\sqrt{\sum_i (x_1(i) - \overline{x}_1)^2}\sqrt{\sum_i (x_2(i) - \overline{x}_2)^2}}.$$

This measures how similar are two temporal series once shifted by a lag τ. On the other hand, phase synchronization is commonly detected by studying the Hilbert phase difference. These two indicators are used in our study to characterize the synchronization between two semiconductor laser outputs. The evaluation of the generalized synchronization requires from more complex techniques. For unidirectional couplings Abarbanel has shown how to detect whether a functional relationship exists between the master and slave systems through an auxiliary system approach[7].
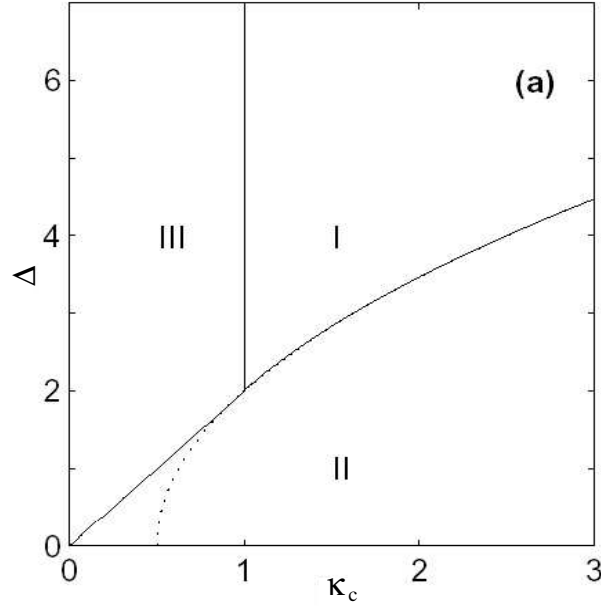
1.3.5   Oscillation quenching

The effect of suppressing the oscillations of interacting systems due to its coupling is known as quenching or oscillation death. The cease of the oscillatory behavior in weakly coupled limit cycle arrays can induce important consequences in both biological and physical systems. In fact, the appearance of this phenomenon in some cell systems seems to be related to severe pathologies such as different types of arrhythmias.

The basics of this effect can be investigated through the study of the two coupled Stuart-Landau equations representing two mutually coupled limit cycles[8]

$$\dot{A}_1 = (1 + i\omega_1 - |A_1|^2)A_1 + \kappa_c(A_2 - A_1) \tag{1.4}$$

$$\dot{A}_2 = (1 + i\omega_2 - |A_2|^2)A_2 + \kappa_c(A_1 - A_2), \tag{1.5}$$

where $A_{1,2}$ represent the complex amplitudes of each system. Exploring the coupling strength (κ_c) versus detuning ($\Delta = \omega_2 - \omega_1$) plane, several dynamical regimes can be obtained as shown in Fig. 2.1. In the figure, the quenching region is limited by the locking and phase drift areas, and it is noticed that a large detuning between the oscillators is needed in order to produce the death effect. Consequently, two identical instantaneously coupled oscillators ($\Delta = 0$) are not allowed to experience a mutual quenching in their oscillations.

Figure 1.1: Dynamical regimes in the coupling vs. detuning plane of two coupled oscillators. I) Quenching region, II) locking area, and III) phase drift zone.

1.4 Delay

1.4.1 Delay differential equations

A fundamental fact in Physics is that any interaction in Nature is not instantaneously transmitted but requires a given time to propagate. Thus, the present state of any system depends on the past of the other systems which is interacting with. This naturally leads to the introduction of a type of functional equations named delay differential equations (DDE's), where the evolution of the variables at time t depend on the variables evaluated at earlier times $t - \tau$. For instance, the retarded potentials in electromagnetism compute the scalar and vector potentials at time t with the charge and current distributions at time $t - r/c$. In vacuum these read

$$V = \frac{1}{4\pi\varepsilon_0} \int_{V'} \frac{\rho(t - r/c)}{r} dV', \quad \mathbf{A} = \frac{\mu_0}{4\pi} \int_{V'} \frac{\mathbf{J}(t - r/c)}{r} dV', \tag{1.6}$$

where ρ and J are the charge and current density, respectively, and r is the distance between the differential of volume (dV') over which the integration is being carried and the point at which the potentials are calculated. When introducing these expressions into the Maxwell and Lorenz equations we end up with a complicated set of equations where the delay $\tau = r/c$ appears inside an integral expression. This kind of differential equations where a variable

is evaluated at a continuum of delay times are known as distributed delay differential equations.

Delay equations also appear in other fields like population dynamics. There, the delays usually arise because of the interest in modeling latency times in the creation of new individuals. A prototypical example of DDE governing the concentration of a given type of cell is the Mackey-Glass equation

$$\dot{x}(t) = -bx(t) + \frac{ax(t-\tau)}{1+x(t-\tau)^{10}}. \tag{1.7}$$

This type of equations where only a finite number of delays appear are called discrete delay differential equations.

Regarding the dimensionality of the phase space described by a set of DDE, it should be noticed that the initial condition needed to univocally solve a DDE is given by the past history of the delayed variables, i.e., $x(t), \forall t \in (-\tau, 0)$. Since this is a continuum of points, the phase space of DDE is infinite-dimensional in the same way that partial differential equations (PDE) are also infinite-dimensional. Another important property that DDE's share with PDE's is the fact that only one equation is needed in order to produce chaotic behavior as opposite to what happens in ordinary differential equations, where at least three coupled equations are required.

The inclusion of such delay times in the interaction between different subsystems is responsible for a series of unexpected behaviors. One of the important examples is the "death by delay" phenomenon by which two identical coupled oscillators can drive each other to a zero-amplitude state by their mutual delayed interaction. This effect was first investigated by Ramana et al.[2] in 1998 through the study of the system of equations

$$\dot{A}_1(t) = (1 + i\omega_1 - |A_1(t)|^2)A_1 + \kappa_c(A_2(t-\tau) - A_1(t)) \tag{1.8}$$

$$\dot{A}_2(t) = (1 + i\omega_2 - |A_2(t)|^2)A_2 + \kappa_c(A_1(t-\tau) - A_2(t)), \tag{1.9}$$

where $A_{1,2}$ represents the complex amplitude of each oscillator and τ is the time delay in the interaction. Fig. 2.2 shows the diagram of the different dynamical states presented in the system. It can be observed that, as opposite to the case of instantaneous coupled oscillators, no necessity of a large detuning is now required in order to observe this quenching, and consequently a delay in the coupling line opens the possibility to observe the oscillation death in coupled identical systems.

The first experimental confirmation of the "death by delay" effect was obtained in 2000 by Herrero and collaborators who studied the dynamics of two mutually coupled thermo-optical cells[4]. To our knowledge we present in this memoire the first experimental confirmation of this effect in a semiconductor laser setup.
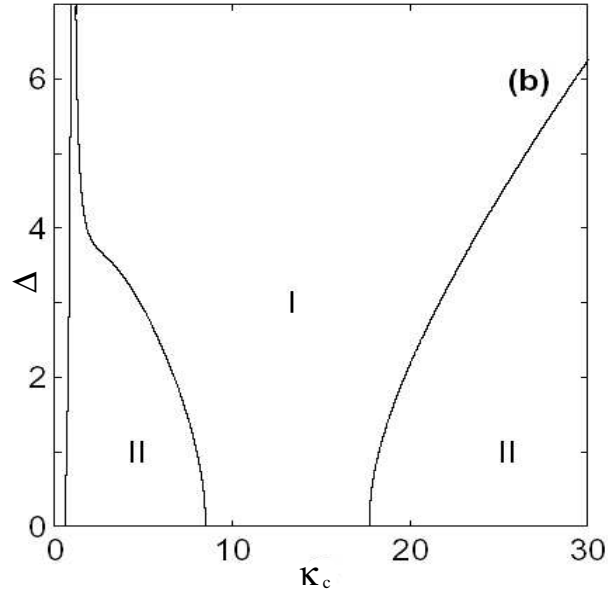
Figure 1.2: Dynamical regimes in the coupling vs. detuning plane of two coupled oscillators. I) Quenching region, II) locking area. The delay is set to $\tau = 10$.

1.4.2 Stability

An important issue in any dynamical system delayed or not is the investigation of the stability of their steady-state solutions or fixed points. To this end let us consider a given system of delay differential equations with discrete delays

$$\dot{\mathbf{x}}(t) = f\left(\mathbf{x}(t), \mathbf{x}(t - \tau_1), ..., \mathbf{x}(t - \tau_m); \mu\right), \tag{1.10}$$

where $x \in \mathbb{R}^n$, f is a function that depends on the instantaneous and delayed variables, and a set of parameters μ. All the delays τ_i we consider here are assumed to be positive.

The linearization of the system 1.10 around a trajectory $\mathbf{x}^*(t)$ leads to the so-called variational equation for the variable $\mathbf{y}(t) = \mathbf{x}(t) - \mathbf{x}^*(t)$,

$$\dot{\mathbf{y}}(t) = A_0(t)\mathbf{y}(t) + \sum_{i=1}^{m} A_i(t)\mathbf{y}(t - \tau_i), \tag{1.11}$$

where,

$$A_i(t) = \frac{\partial f}{\partial \mathbf{x}(t - \tau_i)}\big|_{(\mathbf{x}^*(t), \mathbf{x}^*(t-\tau_1), ..., \mathbf{x}^*(t-\tau_m); \mu)}. \tag{1.12}$$

When $\mathbf{x}^*(t) = \mathbf{x}^*$ correspond to an steady-state, an exponential ansatz for $\mathbf{y}(t)$ leads the so-called characteristic equation,

$$det\left(A_0 + \sum_{i=1}^{m} A_i e^{(-\lambda\tau_i)} - \lambda I\right) = 0. \tag{1.13}$$

The roots or eigenvalues λ of Eq. 1.13, which in general take complex values, rule the stability of the fixed point $\mathbf{x}^*$. The stability criteria reads that if any root have positive real part, then the steady state is unstable. Only when all the eigenvalues are on the left half plane of the complex plane, the fixed point is asymptotically stable. The determination of the stability of a given fixed point can be performed in different ways. These include the analytical or numerical computation of the roots of Eq. (1.13), the use of complex integration for detecting unstable eigenvalues, or the finding of Lyapunov-Krasovkii potentials. In this memoire we restrict ourselves to the analytical and numerical study of the roots distribution because it can provide us much more information. In fact, from an study of how the eigenvalues λ get unstable when a given parameter is continuously changed, a lot of insight about the dynamical system can be gained. This is one of our main goals that can be achieved through the bifurcation theory whose most basic concepts are presented in the next section.

1.5   Basics of bifurcations

In this section we just attempt to review, without any kind of detail, some of the most common bifurcations that appear in a dynamical system like Eq. (1.10). Only local bifurcations of fixed points are considered here since they are the only type of bifurcations we are interested in through all this work.

Let us start by defining what we understand by local bifurcation. For bifurcation we mean a qualitative change in the asymptotic solutions of a dynamical system when some parameter is continuosly changed. These are usually related to the change of stability of existing objects or the birth and death of asymptotic solutions. When the characterization of such a bifurcation can be reduced to the study of a vicinity of a single point in the phase space, the bifurcation is said to be local, otherwise it is qualified as global. The identification of the type of bifurcation a fixed point undergoes can be achieved by looking at how the eigenvalues λ of the characteristic equation cross the imaginary axis as some parameter is varied. Moreover, the symmetry of the dynamical system will impose some restrictions on the type of bifurcation we can find.

First, we begin by describing some basic bifurcations of codimension one. These are bifurcations where only one parameter is needed to be changed in order to meet the bifurcation point.

- **Saddle-node**. In this bifurcation a pair of fixed points (one attracting and one unstable) appear simultaneously as a single control parameter μ passes a threshold μ_0. Near the bifurcation, the distance between the newly created steady-states scales as $(\mu - \mu_0)^{1/2}$. When the bifurcation occurs at μ_0, a real zero eigenvalue crosses the imaginary axis.

- **Transcritical**. It occurs when one stable and one unstable fixed point collide at the bifurcation point μ_0 and interchange their stability. After the bifurcation occurs, the separation of the two fixed points varies linearly with $\mu - \mu_0$. A real zero eigenvalue is also crossing the imaginary axis at the bifurcation point.

- **Pitchfork**. As some control parameter is changed we pass from a single stable fixed point to a situation where three fixed points are produced. In the supercritical (subcritical) version of this bifurcation, the two new steady-states are born stable (unstable) meanwhile the old fixed point gets unstable. It is important to mention that this type of bifurcation only appears in dynamical systems with an appropriate symmetry. A real zero is crossing the imaginary axis at the bifurcation point μ_0. When instead of fixed points the bifurcating structures are limit cycles, the phenomenom in named as spontaneous symmetry-breaking bifurcation. This is due to the fact that in this bifurcation, the limit cycle that losses the stability is symmetric under the symmetry of the dynamical system, while the two new limit cycles created are asymmetric ones.

- **Hopf**. In the supercritical Hopf bifurcation, a previously stable fixed point becomes unstable and a stable limit cycle is born. In the subcritical case, the stable fixed point collides with an existing unstable limit cycle at the bifurcation point and as a consequence the steady-state losses its stability. In this type of bifurcations, the amplitude of the limit cycles that is born at the bifurcation point grows as the square root of the distance of the control parameter to the bifurcation point, i.e., $(\mu - \mu_0)^{1/2}$. The fixed point that is involved in the bifurcation gets unstable when a complex conjugate pair of eigenvalues cross the imaginary axis in the complex plane. The imaginary part of these eigenvalues $\lambda = \pm i\omega$ gives the angular frequency of oscillation of the periodic solution or limit cycle newly created.

As we have seen, the three first types of bifurcations we have commented occur through the unstabilization of a real zero that crosses the imaginary axis. The symmetries and other constrains are the key elements when distinguishing which of the three bifurcations occurs.

Some codimension-two bifurcations, i.e., two control parameters need to be simultaneously varied in order to meet the bifurcation point, are reviewed

below. These bifurcations are sometimes interpreted as the collision or intersection of two codimension-one bifurcations. In the following the list the next three types of bifurcations because they are explicitely encountered in the study of our setup,

- **Takens-Bogdanov**. In this bifurcation, a simple real eigenvalue and a a pure imaginary pair, simultaneously cross to the real positive plane. The unfolding, this is the characterization of the dynamical regimes in the vicinity of the bifurcation point, has been shown to be extremely rich in this kind of bifurcation.

- **Gavrilov-Guckenheimer**. They are identified by a double zero of the characteristic equation. Then, two colliding zero eigenvalues crossing the imaginary axis is the hallmark of this qualitative change in the phase space. This bifurcation is usually interpreted as an accumulation point of a Hopf bifurcation branch, i.e., a point in a family of Hopf bifurcation where the imaginary part of the eigenvalues tends to zero.

- **Hopf-Hopf**. The intersection of two families of Hopf bifurcation lead to this type of codimension two bifurcation, where two complex conjugate imaginary eigenvalues are simultaneously becoming unstable. As in the other codimension-two examples, a lot of different dynamical states appear in the neighborhood of this bifurcating point.

Chapter 2

Results

2.1 The system

THE system under study in this work consists of two semiconductor lasers mutually coupled. However, there are different ways we can choose in order to couple or link the dynamics of two semiconductor lasers (see Fig. 2.1). One of the most popular is the coherent optical coupling, which consists of the injection of the light coming from a laser into the active region of other laser, assuming a coherent interaction between the injected and the intracavity fields. This kind of interaction in master-slave or unidirectional schemes has been found very useful in applications such as frequency stabilization or secure communications. On the other hand, in the incoherent optical coupling, the light being injected into the laser active region does not interfere with the intracavity field, and that injection is only supposed to decrease the level of available carriers. This type of interaction is usually achieved by injecting light with an orthogonal polarization to the junction plane of the laser being injected, since two fields with orthogonal polarization cannot interfere. Finally, in the optoelectronic interaction, the light from a laser is converted into photocurrent and this electronic flow is used to drive the bias current of the other laser. This latter type of interaction (optoelectronic) is the one studied here.

In order to study synchronization in our mutually coupled system of semiconductor lasers, we pointed out in the former chapter that it is very important that when isolated both systems should exhibit a certain type of dynamics by themselves. However, when uncoupled a semiconductor laser operates in steady-state emission for the intensity (the oscillating electric field $E(t)$ is not a variable of our problem since due to the optoelectronic nature of the coupling only the intensity $|E|^2$ is relevant). Consequently, if we want to study the synchronization properties of our two laser system, we need to perturb each solitary laser in order to excite a certain type of dynamics before we couple them. We found that a very convenient way to do so consists of introducing a feedback loop for each semiconductor laser. Here, the feedback loop is also
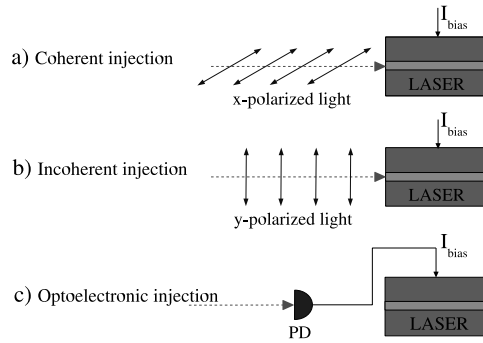
Figure 2.1: Scheme of the different types of injection for a semiconductor laser.

chosen to be of optoelectronic nature, and consequently part of the light extracted from a laser is converted in photocurrent and injected into its own current supply. With the addition of a feedback loop we gain an extraordinary control and tunability on the dynamics of each laser when isolated. For example, by changing the feedback strength and length, we are able to switch from constant, oscillatory, pulsating, or even chaotic behavior.

Consequently, we consider the system sketched in Fig. 2.2, composed by two identical single-mode distributed feedback semiconductor lasers subject to optoelectronic coupling and feedback. This setup corresponds to the experimental situation described in Ref. [9]. The optical power emitted by each laser is detected, amplified, and added to the bias current of its counterpart (optoelectronic coupling) and to its own injection current (optoelectronic feedback). These contributions of the feedback and mutual interaction photocurrents are delayed due to the finite propagation time of the optical and electrical signals.

The dynamics of the photon and carrier densities in each laser is described by the single-mode semiconductor laser rate equations appropriately modified in order to include the coupling and feedback terms. The bidirectional optoelectronic coupling is accounted for by adding, in the carrier rate equations, the delayed photocurrent generated by a laser into the injection current of its counterpart. In a similar way, the effect of the optoelectronic feedback loops is taken into account in each laser by adding to the bias current the delayed photocurrent generated by itself.

The optical phase does not play any role due to the insensitivity of the photodetectors to the phase of the electrical field. Hence, the rate equations for the evolution of the photon and carrier densities in both lasers read [10]
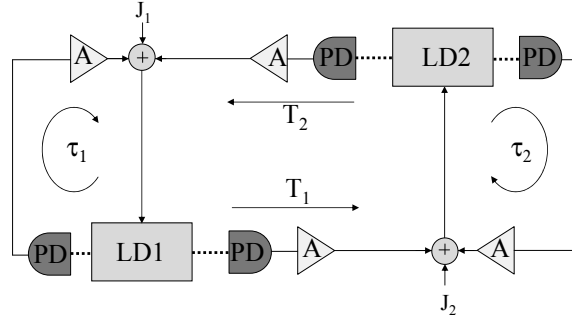
Figure 2.2: Scheme of two lasers subject to optoelectronic feedback and mutual coupling. LD: laser diode; PD: photodetector; A: electrical amplifier.

$$\frac{dS_1}{dt} = -\gamma_{c_1}S_1 + \Gamma g_1 S_1 \tag{2.1}$$

$$\frac{dN_1}{dt} = \frac{J_1}{ed} + \xi_{f_1}S_1(t - \tau_{f1}) + \xi_{c_1}S_2(t - \tau_{c1}) \tag{2.2}$$

$$-\gamma_{s_1}N_1 - g_1 S_1 \tag{2.3}$$

$$\frac{dS_2}{dt} = -\gamma_{c_2}S_2 + \Gamma g_2 S_2 \tag{2.4}$$

$$\frac{dN_2}{dt} = \frac{J_2}{ed} + \xi_{f_2}S_2(t - \tau_{f2}) + \xi_{c_2}S_1(t - \tau_{c2}) \tag{2.5}$$

$$-\gamma_{s_2}N_2 - g_2 S_2, \tag{2.6}$$

where $S_{1,2}$ is the intracavity photon density, $N_{1,2}$ is the carrier density, and $g_{1,2}$ is the material gain. The subindices 1,2 distinguish between the two lasers. $\xi_{c1,2}$ ($\xi_{f1,2}$) stand for the coupling (feedback) strengths, which are proportional to the responsivity of the photodetectors and the amplification factor of the respective amplifiers. $T_{1,2}$ ($\tau_{1,2}$) are the coupling (feedback) delay times. Other parameters appearing in the rate equations are the bias current density J, the cavity decay rate γ_c, the spontaneous carrier relaxation rate γ_s, the confinement factor of the laser waveguide Γ, the electron charge e, and the active layer thickness d. For simplicity, spontaneous emission noise sources have been neglected. It is also important to note that an infinite bandwith photodetector-amplifier response is assumed.

Numerical calculations and experimental measurements show that, in a wide operation range, the material gain has a linear dependence on both the carrier and photon densities. Therefore, $g(N, S)$ is expanded as

$$g \approx g_0 + g_n(N - N_0) + g_p(S - S_0), \tag{2.7}$$

where $g_0 = \gamma_c/\Gamma$ is the material gain at the solitary threshold, $g_n = \partial g/\partial N > 0$ is the differential gain parameter, $g_p = \partial g/\partial S < 0$ is the nonlinear gain parameter, N_0 is the carrier density at threshold, and S_0 is the free-running intracavity photon density when the lasers are decoupled from feedback or mutual interactions. The parameters g_n and g_p are taken to be approximately constants.

After introducing Eq. (2.7) into Eqs. (2.1)-(2.6) and defining the dimensionless variables $\tilde{s} \equiv (S - S_0)/S_0$, $\tilde{n} \equiv (N - N_0)/N_0$, $\tilde{J} = (J/ed - \gamma_s N_0)/\gamma_s N_0$ and $\kappa_c \equiv \xi_c \Gamma/\gamma_c$, and $\kappa_f \equiv \xi_f \Gamma/\gamma_c$, the rate equations read

$$\frac{d\tilde{s}_1}{dt} = \frac{\gamma_{c_1}\gamma_{n_1}}{\gamma_{s_1}\tilde{J}_1}\tilde{n}_1(\tilde{s}_1 + 1) - \gamma_{p_1}\tilde{s}_1(\tilde{s}_1 + 1), \tag{2.8}$$

$$\frac{d\tilde{n}_1}{dt} = \frac{\gamma_{s_1}\gamma_{p_1}}{\gamma_{c_1}}\tilde{J}_1\tilde{s}_1(1 + \tilde{s}_1) + \gamma_{s_1}\kappa_{f_1}\tilde{J}_1\left[1 + \tilde{s}_1(t - \tau_1)\right] + \gamma_{s_1}\kappa_{c_1}\tilde{J}_1\left[1 + \tilde{s}_2(t - T_2)\right]$$
$$-\gamma_{s_1}\tilde{n}_1 - \gamma_{s_1}\tilde{J}_1\tilde{s}_1 - \gamma_{n_1}\tilde{n}_1(1 + \tilde{s}_1), \tag{2.9}$$

$$\frac{d\tilde{s}_2}{dt} = \frac{\gamma_{c_2}\gamma_{n_2}}{\gamma_{s_2}\tilde{J}_2}\tilde{n}_2(\tilde{s}_2 + 1) - \gamma_{p_2}\tilde{s}_2(\tilde{s}_2 + 1), \tag{2.10}$$

$$\frac{d\tilde{n}_2}{dt} = \frac{\gamma_{s_2}\gamma_{p_2}}{\gamma_{c_2}}\tilde{J}_2\tilde{s}_2(1 + \tilde{s}_2) + \gamma_{s_2}\kappa_{f_2}\tilde{J}_2\left[1 + \tilde{s}_2(t - \tau_2)\right] + \gamma_{s_2}\kappa_{c_2}\tilde{J}_2\left[1 + \tilde{s}_1(t - T_1)\right]$$
$$-\gamma_{s_2}\tilde{n}_2 - \gamma_{s_2}\tilde{J}_2\tilde{s}_2 - \gamma_{n_2}\tilde{n}_2(1 + \tilde{s}_2), \tag{2.11}$$

where the differential and nonlinear carrier relaxation rates are defined as $\gamma_n \equiv g_n S_0$ and $\gamma_p \equiv -\Gamma g_p S_0$, respectively. It is worth noting that since $S_0 = \tilde{J}\gamma_s N_0 \Gamma/\gamma_c$, both γ_n and γ_p are related to the bias current. The values of the parameters are those used in Ref. [10], i.e., $\gamma_c = 2.4 \times 10^{11}$ s^{-1}, $\gamma_s = 1.458 \times 10^9$ s^{-1}, $\gamma_n = 3\tilde{J} \times 10^9$ s^{-1}, and $\gamma_p = 3.6\tilde{J} \times 10^9$ s^{-1}. The relaxation oscillation frequency is calculated as $f_r = \frac{1}{2\pi}(\gamma_c\gamma_n + \gamma_p\gamma_s)^{1/2}$, and the dimensionless coupling and feedback strengths read

$$\kappa_{c,f} = a_{c,f}\frac{\eta c\alpha_m\Gamma}{2n_g\gamma_c}\eta_{ext} , \tag{2.12}$$

$a_{c,f}$ being the coupling and feedback amplifier multiplication factors, respectively, η the quantum efficiency of the photodetectors, η_{ext} a parameter that takes into account additional external losses, c the speed of light in vacuum, α_m are the laser facet losses and n_g the group refractive index. For a typical case ($\eta = 0.5$, $\eta_{ext} = 1$, $\alpha_m = 48$ cm^{-1}, $n_g = 3.5$, $\gamma_c = 0.24$ ps^{-1} and $\Gamma = 0.3$) $\kappa_{c,f}$ is of the order of ~ 0.1, when $a_{c,f}$ is fixed to 1. Then, the magnitude of κ_c (or κ_f) can be easily modified just by changing the corresponding amplification factor or the external attenuation. In addition, the sign of κ_c (or κ_f) can be reversed by subtracting the generated photocurrent from the bias instead of adding it. In this paper, we consider both positive and negative values for the coupling and feedback strengths.

2.2 Stability and bifurcation analysis

As usual in nonlinear dynamical systems, a bifurcation study of the fixed points or equilibria allows us to collect a great deal of information about the different dynamical regimes that can rise in the setup under investigation. In this section, we locate and discuss the stability of the fixed points of the system of Eqs. (2.8)-(2.11). We analyze the role of the different coupling strengths and delay times and construct several stability diagrams.

For the sake of clarity, we reduce the number of free parameters by assuming two device-identical lasers under symmetric operation. Hereafter, we assume identical bias currents ($\tilde{J}_1 = \tilde{J}_2 \equiv \tilde{J}$), coupling strengths ($\kappa_{c_1} = \kappa_{c_2} \equiv \kappa_c$), feedback strengths ($\kappa_{f_1} = \kappa_{f_2} \equiv \kappa_f$), and feedback loop delays ($\tau_1 = \tau_2 \equiv \tau$). These approximations are realistic due to the large degree of symmetry of the lasers used in the experiments [9]. Moreover, it is well known that this kind of degenerate conditions give rise to the organizing centers of the dynamics. For the numerical examples given in this section the bias current taken is $\tilde{J} = 1/3$.

2.2.1 Location of fixed points

The conditions we impose to find the fixed points are $\tilde{s}_1(t) = \tilde{s}_{1st}$, $\tilde{s}_2(t) = \tilde{s}_{2st}$, $\tilde{n}_1(t) = \tilde{n}_{1st}$, and $\tilde{n}_2(t) = \tilde{n}_{2st}$, which provide four different fixed points. The first solution (FP1), $\tilde{s}_{1st} = -1$, $\tilde{n}_{1st} = \tilde{J}$, $\tilde{s}_{2st} = -1$, and $\tilde{n}_{2st} = \tilde{J}$, defines the "OFF" state of the lasers. When operating in this fixed point neither laser is emitting light from their facets. There exist two additional fixed points (FP2 and FP3), which correspond to the case in which one laser is emitting while the other is switched-off. These solutions represent the two possible asymmetric steady states. The solution for the F.P. 2 is

$$
\begin{aligned}
\tilde{s}_{1st} &= \frac{\kappa_f \gamma_c \gamma_n}{\gamma_c \gamma_n (1 - \kappa_f) + \gamma_p \gamma_s}, \\
\tilde{n}_{1st} &= \tilde{J} \frac{\gamma_p \gamma_s}{\gamma_c \gamma_n} \tilde{s}_{1st}, \\
\tilde{s}_{2st} &= -1, \\
\tilde{n}_{2st} &= \tilde{J} \left(1 + \kappa_c + \kappa_c \tilde{s}_{1st} \right),
\end{aligned}
\tag{2.13}
$$

while the solution for the F.P. 3 is obtained by simply interchanging the subindices 1 and 2. Finally, the steady-state conditions allow for one more fixed point defining the "ON" state of both lasers (F.P. 4):

$$
\begin{aligned}
\tilde{s}_{1st} &= \tilde{s}_{2st} = \frac{(\kappa_c + \kappa_f) \gamma_c \gamma_n}{(1 - \kappa_c - \kappa_f) \gamma_c \gamma_n - \gamma_p \gamma_s}, \\
\tilde{n}_{1st} &= \tilde{n}_{2st} = \tilde{J} \frac{\gamma_p \gamma_s}{\gamma_c \gamma_n} \tilde{s}_{1st}.
\end{aligned}
\tag{2.14}
$$

The first goal we focus on is the construction of the stability charts associated to the different fixed points. We mainly study the stability diagrams in the coupling versus feedback strength plane (κ_c vs. κ_f), and in the coupling time versus feedback time plane (T vs. τ). A detailed analysis of the bifurcations will directly lead us to the construction of such stability diagrams.

In general this bifurcation study can be performed through the computation of the eigenvalues λ of the characteristic equation of system Eqs. (2.8)-(2.11) $z(\lambda, \mu) = 0$, once linearized around a fixed point, as a function of a given set of parameters μ.

We proceed by locating in the parameter space spanned by κ_c, κ_f, τ, and $T \equiv (T_1 + T_2)/2$ different types of bifurcations. We remark that T is the relevant bifurcation parameter instead of T_1 and T_2 since only the sum of these delays appear the characteristic equation [11].

2.2.2 Stability of the symmetric fixed point FP1

First, we treat the stability of FP1, which can only be destabilized through a real eigenvalue. It can be analytically demonstrated from the characteristic equation that the FP1 losses its stability at exactly the same bias current than in the solitary case. That is, both have the same threshold ($\tilde{J} = 0$). This fact agrees with the naive interpretation that threshold reduction in semiconductor lasers subject to optical injection or feedback, only occurs though the coherent interaction of the intracavity and injected fields. From the fixed point picture, the loss of stability of FP1 occurs through a transcritical bifurcation when FP1 collides with FP4.

2.2.3 Stability of the symmetric fixed point FP4

For the other symmetric steady state (FP4), we separate the cases where a real or complex eigenvalues are crossing the imaginary axis.

Real eigenvalues

The analysis of the characteristic equation yields the condition to obtain a real zero eigenvalue ($\lambda = 0$) as

$$\kappa_c - \kappa_f = -1 - \frac{\gamma_p \gamma_s}{\gamma_c \gamma_n}. \tag{2.15}$$

This leads to the condition that inside the region defined by the inequality $\kappa_c - \kappa_f < -1 - \gamma_p \gamma_s / \gamma_c \gamma_n$ in the coupling versus feedback strengths plane, there is at least one eigenvalue of FP4 with a positive real part, and consequently the fixed point is unstable. We notice that this condition is independent on the time delays, that is to say, regardless of the values of T and τ the simultaneous constant-wave (CW) operation of both lasers is unstable.

While discussing the transition of real eigenvalues to the right hand side of the complex plane, we can take advantage and analyze a codimension-two kind of bifurcation known as the Takens-Bogdanov bifurcation. The Takens-Bogdanov (TB) points are found by demanding a double zero root of the characteristic equation ($z(\lambda) = \partial z / \partial \lambda = 0$). These points must simultaneously fulfill Eq. (2.15) ($z(\lambda) = 0$) in addition to the following relationship ($\partial z / \partial \lambda = 0$)

$$\begin{aligned}
&\gamma_p \gamma_s (\gamma_n + \gamma_p + \gamma_s) + \kappa_f \gamma_c^2 \gamma_n^2 \tau + \\
&\gamma_c \gamma_n \left[\gamma_n + \gamma_p + (1 - \kappa_c - \kappa_f) \gamma_s + \kappa_f \gamma_p \gamma_s \tau) \right] \\
&= T \kappa_c \gamma_c \gamma_n (\gamma_c \gamma_n + \gamma_p \gamma_s).
\end{aligned} \tag{2.16}$$

In order to locate the TB points, we may fix a value for κ_f, whereas κ_c is obtained from Eq. (2.15). For κ_f and κ_c given, Eq. (2.16) provides a linear relationship between the two time delays τ and T. Moreover, we have to impose the physical requirement of the positiveness of the time delays involved in such codimension-two points. Once one of the bifurcation points is located we know from previous studies[12] that very rich dynamical regimes exist in the vicinity of that point, such as the phenomenon of excitability. We also notice that the nature of this codimension-two bifurcation points as an accumulation point of a Hopf curve has been numerically checked.

Complex eigenvalues

A bit more complicated than the previous case is the detection of bifurcations involving complex eigenvalues. We can use different approaches for locating bifurcations in DDE's. Recently, a Matlab package[13] has been developed in order to study the bifurcations of fixed points and limit cycles in DDE's by using numerical techniques on the characteristic equation and monodromic equation for steady-states and periodic orbits, respectively. Another possibility is just to numerically explore the parameter space under study and try to identify the different dynamical regimes. However, when possible, is always better the use of exact computations which lead to analytical criteria. To our purposes, we make use of both analytical techniques and extensive numerical simulations.

Let us begin by writing down the characteristic equation for the FP4. Due to the symmetric solution we are considering, where both lasers are identical and the system equations exhibit a clear $\mathbb{Z}_2$-symmetry (we can interchange laser 1 and 2), the characteristic equation factorize as follows

$$\left(u e^{-\lambda \tau} + p \lambda^2 + q \lambda + y - v e^{-\lambda T} \right) \left(u e^{-\lambda \tau} + p \lambda^2 + q \lambda + y + v e^{-\lambda T} \right) = 0, \tag{2.17}$$

where u, v, p, q, and r involved coefficients that depend on κ_c, κ_f, and $\tilde{J}$. We start by considering the zeroes of the two factors of equation 2.17 after

imposing pure imaginary eigenvalues $\lambda = i\omega$. Then, the eigenfrequencies must satisfy the equation

$$ue^{-i\omega\tau} - p\omega^2 + iq\omega + y \mp ve^{i\omega T} = 0, \tag{2.18}$$

which is divided in real and imaginary parts as follows

$$u\cos\omega\tau - p\omega^2 + y = \pm v\cos\omega T = 0 \tag{2.19}$$

$$-u\sin\omega\tau + q\omega = \mp v\sin\omega T = 0, \tag{2.20}$$

from where it is easy to eliminate the coupling delay time T after squaring and adding Eqs. (2.19)-(2.20). After this, the resulting equation for ω reads

$$\omega^4 + b\,\omega^2 + c + (d\,\omega^2 + e)\cos(\omega\tau) + f\,\omega\sin(\omega\tau) = 0, \tag{2.21}$$

where the coefficients are involved functions of the parameters

$$
\begin{aligned}
b\Lambda^2 =\ & 2\left(-1 + \kappa_c + \kappa_f\right)\gamma_c{}^3\gamma_n{}^3 + \gamma_p{}^2\gamma_s{}^2\left((\gamma_n + \gamma_p)^2 + 2\,\gamma_n\,\gamma_s + \gamma_s{}^2\right) \\
& + 2\,\gamma_c\,\gamma_n\,\gamma_p\,\gamma_s\left((\gamma_n + \gamma_p)^2 - \left((-2 + \kappa_c + \kappa_f)\,\gamma_n + \gamma_p\right)\gamma_s - (-1 + \kappa_c + \kappa_f)\,\gamma_s{}^2\right) \\
& + \gamma_c{}^2\gamma_n{}^2\left((\gamma_n + \gamma_p)^2 - 2\left((-1 + \kappa_c + \kappa_f)\,\gamma_n - (-2 + \kappa_c + \kappa_f)\,\gamma_p\right)\gamma_s\right. \\
& \left. + (-1 + \kappa_c + \kappa_f)^2\,\gamma_s{}^2\right), \\
c\Lambda^2 =\ & -\left((\gamma_c\,\gamma_n + \gamma_p\,\gamma_s)^2\left((-1 + \kappa_c{}^2 - \kappa_f{}^2)\,\gamma_c{}^2\gamma_n{}^2 - 2\,\gamma_c\,\gamma_n\,\gamma_p\,\gamma_s - \gamma_p{}^2\gamma_s{}^2\right)\right), \\
d\Lambda =\ & -2\,\kappa_f\,\gamma_c\,\gamma_n\left(\gamma_c\,\gamma_n + \gamma_p\,\gamma_s\right), \\
e\Lambda^2 =\ & -2\,\kappa_f\,\gamma_c\,\gamma_n\left(\gamma_c\,\gamma_n + \gamma_p\,\gamma_s\right)^3, \\
f\Lambda^2 =\ & -2\,\kappa_f\,\gamma_c\,\gamma_n\left(\gamma_c\,\gamma_n + \gamma_p\,\gamma_s\right)\left(-\left(\gamma_c\,\gamma_n\left(\gamma_n + \gamma_p\right)\right) + (-1 + \kappa_c + \kappa_f)\,\gamma_c\,\gamma_n\,\gamma_s\right. \\
& \left. - \gamma_p\,\gamma_s\left(\gamma_n + \gamma_p + \gamma_s\right)\right), \\
\Lambda \equiv\ & (-1 + \kappa_c + \kappa_f)\,\gamma_c\,\gamma_n - \gamma_p\,\gamma_s\,.
\end{aligned}
$$

Then, in order to construct the stability diagram of FP4 it is of central importance to determine the regions in the coupling versus feedback plane where a real solution for Eq. (2.21) exists. The set of points in the κ_c vs. κ_f plane where no real solution for ω exists regardless the delay times τ and T, is called the delay independent stable region (DISR). Consequently, within that region any possible combination of feedback and coupling delay times is unable to destabilize the CW emission of the lasers on the FP4. On the contrary, there also exists some points of in the κ_c vs. κ_f plane where the existence of a real solution for ω depends on the specific values of the feedback and coupling delay times. Such a zone is the delay-dependent stable region

(DDSR), and there one can always find a proper combination of delay times that induces oscillations through a Hopf bifurcation. Finally, we can define the delay independent unstable region (DIUR), where no matter the delay times we chose the system is unstable when operating on FP4. In this case, the condition given in Eq. (2.15) defines an area where an eigenvalue with positive real part exists independently of τ and T, and as a consequence FP4 is unstable.

To the purpose of finding the before-mentioned regions, we will not solve the transcendent equation (2.21) by numerical methods. Instead, we will be able to find analytical conditions on its coefficients. Let us consider the left-hand side of Eq. (2.21) as a function of the two variables ω and τ. Then, once fixed κ_c and κ_f, we need to scan the plane ω versus τ and check whether at least a real root of the Eq. (2.21) exists. If no zero can be found we can assure that the values used for κ_c and κ_f correspond to a DISR point because independently of τ and T no Hopf instability can perturb FP4. On the other hand, if such a zero is found, the Hopf bifurcation is obtained for a precise value of the coupling and feedback times and the stability of FP4 becomes delay dependent (DDSR). The only exception to the former discussion is produced when dealing with values of κ_c and κ_f that fall inside the DIUR zone described by Eq. (2.15). There, FP4 is unstable independently whether we found a zero of Eq. (2.21) because a real eigenvalue has already crossed the imaginary axis and become unstable.

In principle, the task of looking for roots should be done by numerical solving Eq. (2.21). However, a clever way to inspect the ω vs. τ plane that can lead us to analytical conditions on the coefficients for the existence of roots, is through the family of hyperbolas $\omega\tau = h = \text{constant}$. On each of these curves, Eq. (2.21) is simply reduced to a fourth-order polynomial, for which the conditions for its coefficients to have no real solutions are known [14, 15, 16]. For each value of h, the polynomial obtained from the left-hand side of Eq. (2.21) is written as $P(\omega) = \omega^4 + r\omega^2 + s\omega + t$. Since we are dealing with fourth order polynomials with real coefficients, the number of real roots of each of these polynomials will be zero, two, or four. Which of these cases occurs can be determined by computing the discriminants of the polynomial from its resultant matrix. After having obtained the following polynomial discriminants from the central minors of the resultant matrix of the polynomial $P(\omega)$ with its derivative $P'(\omega)$ [17]

$$
\begin{aligned}
\Delta_1 &= 1, \\
\Delta_2 &= -r, \\
\Delta_3 &= -2r^3 - 9s^2 + 8rt, \\
\Delta_4 &= -4r^3s^2 - 27s^4 + 16r^4t + 144rs^2t \\
&\quad -128r^2t^2 + 256t^3,
\end{aligned}
$$

the conditions on the coefficients for obtaining a given number of roots is collected in Table 2.1.

Table 2.1: Real zeroes of a quartic polynomial.

Number of real roots	Multiplicity	Discriminant conditions
0	0	$\Delta_4 > 0 \cap (\Delta_3 \leq 0 \cup \Delta_2 \leq 0)$
0	0	$(\Delta_4 = \Delta_3 = 0) \cap \Delta_2 < 0$
2	1,1	$\Delta_4 < 0$
2	2	$\Delta_3 < 0 \cap \Delta_4 = 0$
4	1,1,1,1	$\Delta_2 > 0 \cap \Delta_3 > 0 \cap \Delta_4 > 0$
4	1,1,2	$\Delta_2 > 0 \cap \Delta_3 > 0 \cap \Delta_4 = 0$
4	2,2	$\Delta_2 > 0 \cap (\Delta_3 = \Delta_4 = 0) \cap s = 0$
4	1,3	$\Delta_2 > 0 \cap (\Delta_3 = \Delta_4 = 0) \cap s \neq 0$
4	4	$\Delta_2 = \Delta_3 = \Delta_4 = 0$

Thus, by varying the value of h from 0 to 2π we can analytically obtain a series of regions in the κ_c vs. κ_f space (remember that these strengths are related to the polynomial coefficients) where no root can be found and consequently provide the delay-independent stable region or DISR zone. Since the DIUR region is determined by the condition given in Eq. (2.15), we obtain the DDSR region as the complementary set to the union of DISR and DIUR. Fig. 2.3 summarize and collects the results concerning the stability of FP4 in the coupling versus feedback strengths.
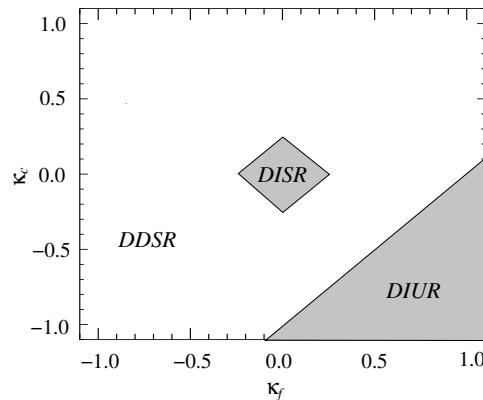
Figure 2.3: Stability diagram in the κ_c vs. κ_f plane for FP4, showing the delay-independent stable region (DISR), the delay-dependent stable region (DDSR), and the delay-independent unstable region (DIUR). The boundary between the DDSR and DIUR defines the transcritical line.

It is important to notice that κ_c and κ_f play a highly symmetrical role when defining the DISR zone. That is, either increasing the magnitude of the coupling or feedback strength we are able to enter into the DDSR regardless the sign of these interactions. However, concerning the DIUR zone it is very important the sign of the strengths considered. For instance, only with a very negative coupling or very large positive feedback we enter into the DIUR zone. So, we see how an inhibitory coupling and an excitatory feedback complement each other in order to destabilize the symmetric FP4. A naive interpretation of the destabilizing role of the inhibitory coupling in our system is that it tends to stablish a kind of competition between both lasers, so a very high negative coupling strength eventually favors the operation in one of the asymmetric states of the system.

So far, we have identified the effect of the different strength constants in the stability of the system, regardless of the specific values that the delay times could take. Next, we fix the coupling and feedback strengths and focus on the role of the delay times. Once a solution of the characteristic equation (2.21) is obtained, the critical coupling delay time T_c for which at least a pair of conjugate eigenvalues lie on the imaginary axis provides the Hopf bifurcation points. We remember that the coupling delay time, which had been eliminated from Eqs. (2.19)-(2.20), can be easily recovered from the same equations. Taking into account the periodicity associated to the coupling delay time T, due to the fact that it only appears as the argument of trigonometric functions, T_c is written down as

$$T_c(\omega) = \frac{1}{\omega} \left(\arctan \frac{g(\kappa_c, \kappa_f, \tau, \omega)}{h(\kappa_c, \kappa_f, \tau, \omega)} + m\pi \right), \tag{2.22}$$

where $m \in \mathbb{Z}$, and g and h are defined by the following expressions

$$\begin{aligned} g &\equiv \left[\gamma_p \gamma_s (\gamma_n + \gamma_p + \gamma_s) + \gamma_c \gamma_n (\gamma_n + \gamma_p - (-1 + \kappa_c + \kappa_f)\gamma_s) \right] \omega \\ &\quad + \kappa_f \gamma_c \gamma_n (\gamma_c \gamma_n + \gamma_p \gamma_s) \sin(\omega\tau), \\ h &\equiv -\gamma_c^2 \gamma_n^2 + \gamma_p \gamma_s (\omega^2 - \gamma_p \gamma_s) - \gamma_c \gamma_n \left[2\gamma_p \gamma_s + (-1 - \kappa_c + \kappa_f)\omega^2 \right] \\ &\quad + \kappa_f \gamma_c \gamma_n (\gamma_c \gamma_n + \gamma_p \gamma_s) \cos(\omega\tau). \end{aligned}$$

The Hopf curves have been calculated in Fig. 2.4 for the case $\kappa_c = \kappa_f = 0.25$. At the intersection of these Hopf curves, we identify the double Hopf codimension-two points where two pairs of purely imaginary conjugate eigenvalues exist.

In order to complete our investigation of codimension-two bifurcations we proceed by locating the Gavrilov-Guckenheimer points (GG) in the parameter space. We recall that in order to detect that type of bifurcations we must demand a single zero eigenvalue in addition to a purely imaginary eigenvalue pair. Hence, we need to satisfy simultaneously the conditions given by Eq. (2.15) and Eq. (2.22). For instance, if we take a feedback
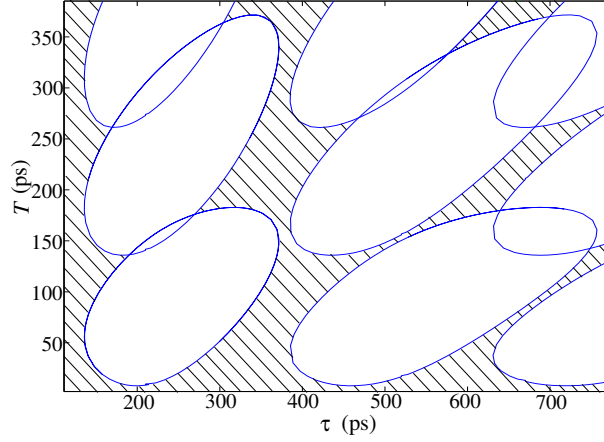
Figure 2.4: Hopf curves and stability diagram in the T vs. τ plane for FP4. The oblique lines indicate the regions where the fixed point is stable. At the crossing of the Hopf curves, a double Hopf codimension-two bifurcation takes place. Both the feedback and coupling strength are fixed at 0.25.

strength κ_f, Eq. (2.15) implies that the coupling strength has to be set to $\kappa_c = \kappa_f - 1 - \gamma_p \gamma_s / (\gamma_c \gamma_n)$. If the feedback delay time is τ, then we obtain from Eq. (2.21) a set of real positive solutions ω_k. If we substitute ω_k into Eq. (2.22), we find a set of coupling delay times T_k associated with each GG point. We can add or subtract multiples of π / ω_k to T_k in order to construct another GG point, although we stress that only positive values of T_k are physically meaningful. As happens with the other codimension-two bifurcation points we detected, the richness of dynamical states that is found around these points is huge.

2.2.4 Stability of the asymmetric fixed points FP2 and FP3

The study of the stability of the asymmetric steady states FP2 and FP3 through the characteristic equation turns out to be challenging for any analytical treatment. Nevertheless, we have undertaken extensive numerical simulation of Eqs. (2.8)-(2.9) for analyzing their stability. The stability charts for FP2 and FP3 are equivalent and presented in Fig. 2.5. The boundary between DIUR and DDSR defines the transcritical line as in Fig. 2.3. However, we note that both regions are interchanged in the figures. Therefore, over that boundary there exists an exchange of the stability between the FP4 and the asymmetric fixed points FP2 and FP3. Moreover, there also exists a small delay-independent stable region (DISR) bounded by the critical line given by Eq. (2.15) on one side, and by the minimum feedback coefficient that is able to excite oscillations in the solitary laser case ($\kappa_f \sim 0.24$), on the other side.

By now we have provided insight into the stability and bifurcation of the
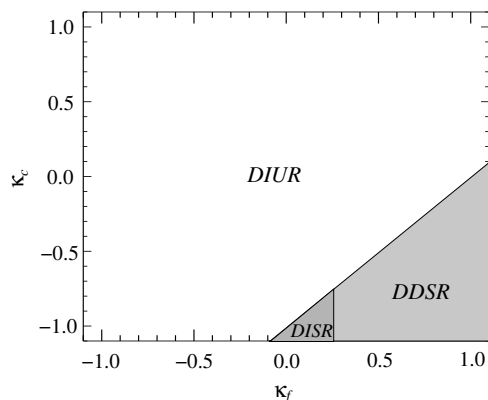
Figure 2.5: Stability diagram in the κ_c vs. κ_f plane for FP2 and FP3, showing the delay-independent stable region (DISR), the delay-dependent stable region (DDSR) and the delay-independent unstable region (DIUR).

steady-states. This analysis will be useful in the next section in order to characterize the "death by delay" phenomenon as well as some general phenomena in the theory of coupled oscillators. The prediction of these phenomena in our laser system allows for a direct translation into observable scenarios and experimental verification.

2.3 Dynamical behavior

In this section, we investigate the dynamical behavior of the lasers acting as two delayed coupled self-sustained oscillators. We address the oscillation death, frequency-locking and synchronization properties.

2.3.1 Death by delay

We use a proper combination of the feedback strength and feedback delay times in order to force each laser to operate as a limit cycle oscillator when uncoupled. Under this situation, we inspect the role of the coupling delay time T in the dynamics. In particular, we investigate the phenomenon of oscillation death, by which the coupling between the two oscillators induces the quenching of the limit cycles through a collapse to the zero amplitude state [2, 9, 8, 18]. When delay is absent in the coupling term, a large dispersion or detuning in the natural frequencies of the oscillators is required to observe this phenomenon, besides the requirement that the coupling must be diffusive [8, 19, 20]. Only recently, Ramana et al. [2] showed that these restrictions can be relaxed if the coupling contains a delay. This effect, commonly known in the literature as "death by delay".

Since the feedback loops are also delayed, we must investigate the role of three parameters, namely, the coupling strength κ_c, and the two delay times T and τ on the oscillation quenching. We tackle the problem by computing the Hopf curves for the FP4 in the κ_c vs. T plane (Eqs. (2.21)-(2.22)), and the direction of transition of the eigenvalues when crossing the imaginary axis.
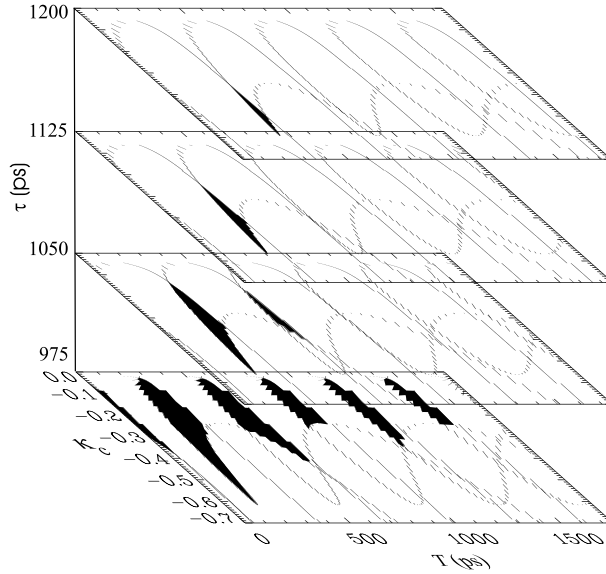
Figure 2.6: Hopf curves and "death islands" (shadowed regions) in the κ_c vs. T plane for FP4 for several values of the feedback delay time. From top to bottom the feedback delays are 1200, 1125, 1050, and 975 ps. The feedback strength and injection current are set at $\kappa_f = 0.3$ and $\tilde{J} = 0.1$, respectively.

Following this procedure, we are able to find closed regions in the parameter space $\kappa_c - T$ where the FP4 is stable, thus inducing the death of the oscillations. These regions surrounded by a supercritical Hopf line are called "death islands". Fig. 2.6 illustrates the location of the "death islands" for $\kappa_f = 0.3$ when the feedback delay time is varied from $\tau = 975$ to $\tau = 1200$ ps. Under these conditions, both lasers oscillate with a fundamental period ~ 600 ps when uncoupled.

For feedback delay times below $\tau = 925$ ps, not shown in the figure, it is meaningless to talk about "death islands" since the lasers are stable even when decoupled. "Death islands start to appear when the solitary lasers undergo self-sustained oscillations at $\tau \sim 950$ ps. Several "death islands" can be observed at the lower panel of Fig. 2.6, computed for $\tau = 975$ ps, which are regularly, although not completely, spaced. The existence of multiple islands when varying T has been experimentally demonstrated [9]. We can observe that the size of these islands decrease when the coupling delay time T increases, until they completely disappear for $T \gtrsim 1500$ ps. The different layers in the figure correspond to different feedback delay times τ. Interestingly, the number of islands and their size continuously decrease when increasing τ,

until they completely disappear for $\tau > 1225$ ps. In summary, we have demonstrated that the "death by delay" phenomenon appears in a wide parameter range in our system. However, we remark that the feedback delay time τ has to be close to a Hopf points of the uncoupled lasers in order to observe this phenomenon.

An interesting feature in Fig. 2.6 is the fact that one of the "death islands" reaches the $T = 0$ axis for the case in which the feedback delay time is set around 975 ps. This fact occurs for feedback delays τ in the range (950-1025) ps. These observations were also independently confirmed by the direct computation of the eigenvalues of the characteristic equation with the MATLAB package for analysis of delay differential equations DDE-Biftool [13]. Therefore, there is an apparent contradiction with the above mentioned arguments that no identical oscillators can drive each other to a zero amplitude state in the absence of delay in the coupling. However, in our setup we do observe the quenching of two identical oscillators even for zero delay in the coupling. The apparent controversy arises from the special origin of the pulsating behavior in our laser system, which is induced by a feedback term with its own delay time. Hence, we conjecture that a delay is necessary in the equations in order to observe the death effect for identically coupled oscillators, regardless of its origin is in the coupling or feedback line. It is worth noting that the preceding studies of "death by delay" [2, 19, 4, 21] considered systems containing time delay in the coupling interaction but no delayed feedback loops were taken into account.

We have analyzed the behavior of the laser outputs when moving into different "death islands". For the case $\tau = 975$ ps and $\kappa_c = -0.2$ in lower panel in Fig. 2.6, we vary the coupling delay from $T = 50$ ps to $T = 0$ ps. In this case, the change in T causes a mutual drift to the zero amplitude state through a series of in-phase pulses with a decreasing exponential envelope. Fig. 2.7
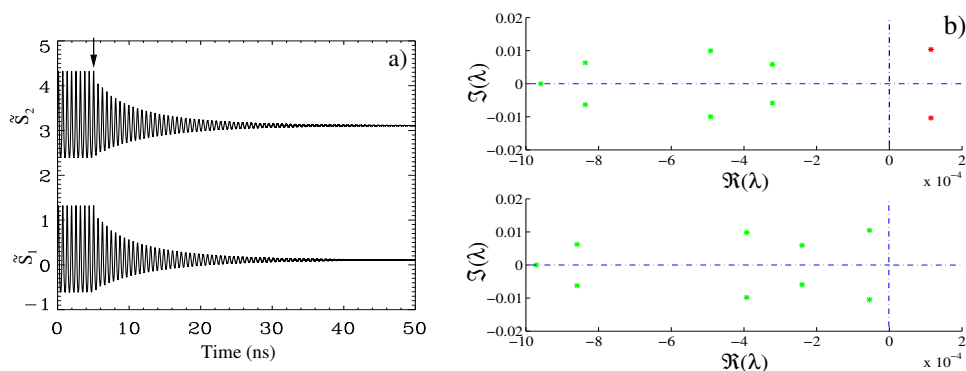
Figure 2.7: (a) Quenching of the oscillations when the coupling delay in changed ($T = 50$ ps $\mapsto T = 0$ ps). The temporal series of laser 2 has been vertically displaced for clearness reasons. (b) Top: eigenvalues at $T = 50$ ps; bottom: eigenvalues at $T = 0$ ps. The bias, feedback coefficient, and feedback delay time correspond to those of the lower panel in Fig. 2.6. The coupling is fixed at $\kappa_c = -0.2$.
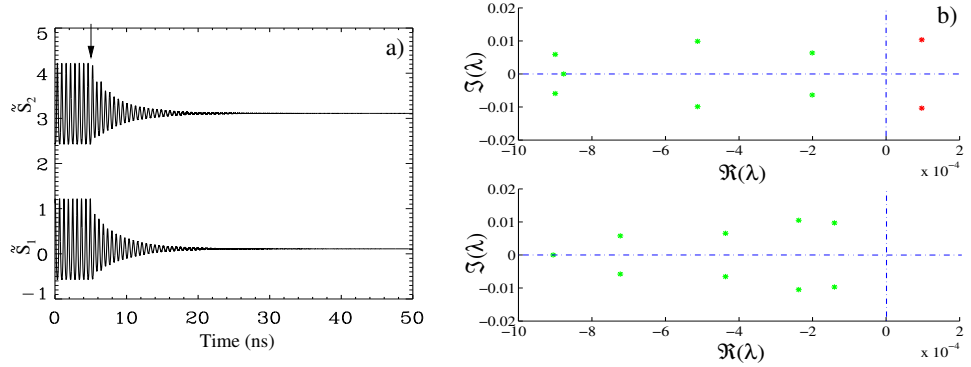
Figure 2.8: (a) Quenching of the oscillations when the coupling delay in changed ($T = 350$ ps $\mapsto T = 250$ ps). The temporal series of laser 2 has been vertically displaced for clearness reasons. (b) Top: eigenvalues at $T = 350$ ps; bottom: eigenvalues at $T = 250$ ps. The bias, feedback coefficient, and feedback delay time correspond to those of the lower panel in Fig. 2.6. The coupling is fixed at $\kappa_c = -0.2$.

Typical "death by delay" quenching was also confirmed when changing the coupling delay time from $T = 350$ ps to $T = 250$ ps, which corresponds to a jump into the second island of lower panel in Fig. 2.6. However, this time the oscillations cease through a series of anti-phase pulses as seen in Fig. 2.8.

The reason for this phase behavior is associated with the formation of phase and anti-phase limit cycles when T increases. We will provide a detailed description of this phenomenon in the next section.

Then the most important result we have obtained in this section is that in order to observe the amplitude quenching effect between coupled oscillators, neither an asymmetry nor a delayed coupling is strictly necessary if the oscillators are subject to a delayed feedback loops.

2.3.2 Synchronization

The entrainment or synchronization between the lasers is studied in three different situations. For identical lasers, we first consider the case of coupled limit cycle oscillators, and secondly we address the synchronization of chaotic oscillators. Finally, we analyze the role of slightly asymmetric operation of the lasers. The different types of synchronization are characterized by two figures of merit, namely, the correlation degree between amplitudes and the relative phase of the oscillations.

2.3.2.a *Identical systems*

Several phenomena related with the synchronization concepts appear in our multiple delayed system. Starting from a configuration in which both lasers are self-sustained oscillators due to their own feedback loop, we study the amplitude and phase synchronization between the laser intensities as a function

of the coupling strength and delay time. The amplitude correlation between the signals is characterized through the maximum of the cross-correlation function, while the phase synchronization is studied by means of the analytical signal concept constructed with the aid of the Hilbert transform [22].
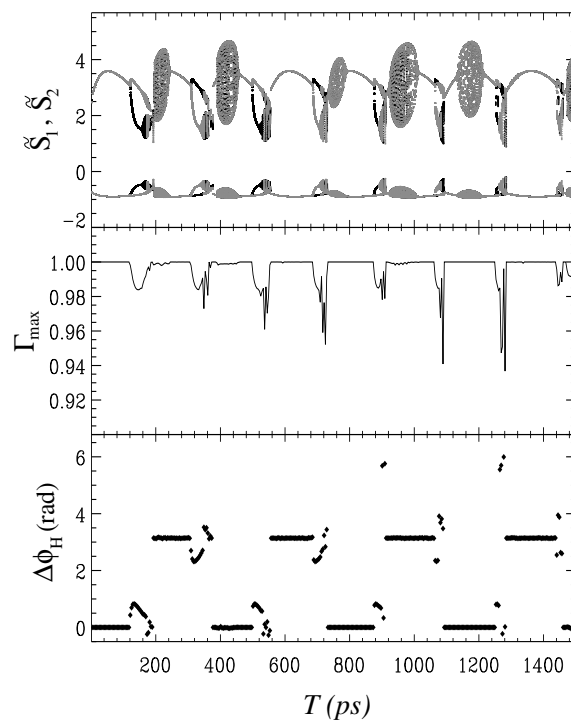
Figure 2.9: Top: bifurcation diagram for $\tilde{s}_1$ (black) and $\tilde{s}_2$ (grey) when changing T. Middle: maximum of the cross-correlation function Γ. Bottom: mean Hilbert phase difference $\Delta\phi_H$. The feedback parameters are $\kappa_f = 0.3$ and $\tau = 1$ ns, while the coupling strength is fixed at $\kappa_c = -0.1$. The bias is set to $\tilde{J} = 1/3$.

First, we describe the different dynamical regimes observed when changing the T. In Fig. 2.9, we show from top to bottom the bifurcation diagram of the laser intensities when T is varied, the maximum of the cross-correlation function, and the mean Hilbert phase difference between the laser signals. Interestingly, we can observe how increasing the coupling delay time a sequence of symmetry-breaking or pitchfork bifurcations for limit cycles occurs. The breaking of the $\mathbb{Z}_2$-symmetry under the interchange of laser 1 and 2 in the Eqs. (2.8)-(2.9) leads to localized synchronization between the two lasers [23, 24]. This is, for instance, observed at $T \sim 120$ ps. Before that point, the two lasers operate in an in-phase symmetric limit cycle and both lasers display oscillations with the same amplitude. After the bifurcation, the system operates in one of the two newly created asymmetric limit cycles, where each laser pulses with a different amplitude but at the same frequency. The localized synchronization is also characterized by a non-zero relative phase

between the two oscillators. By continuing the delay coupling time these asymmetric limit cycles bifurcate to a torus and a quasi-periodic dynamics with different amplitude is observed for each laser. Further increasing the bifurcation parameter a transition to a more complex behavior occurs, where both lasers show irregular oscillations with similar amplitudes and exhibit an anti-phase dynamics. We observe how for larger delays the system tends to operate in an anti-phase limit cycle and further increasing of T this limit cycle undergoes the same type of bifurcations than the ones commented for the previous in-phase limit cycle. This kind of structure going from an in-phase limit cycle to an anti-phase limit cycle and vice versa is repeated as T increases, and consequently several islands of localized synchronization, quasi-periodic dynamics, and in-phase and anti-phase pulsating behavior are found. A plot of the symmetric and the two asymmetric limit cycles created at the pitchfork bifurcation that occurs at $T \sim 500$ ps is shown in Fig. 2.10.
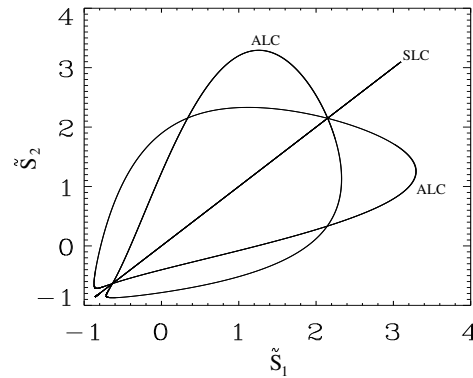

Figure 2.10: Portrait of the limit cycles involved in the spontaneous symmetry-breaking bifurcation. SLC and ALC stand for symmetric limit cycle and asymmetric limit cycle, respectively. The SLC is plotted when is still stable at $T = 496$ ps, while the ALC are showed just after the bifurcation takes place at $T = 498$ ps.

Then, and depending on the initial conditions, the perfectly symmetric system spontaneously tends to operate in one or other of the asymmetric limit cycles. The point here is that in either of these asymmetric limit cycles, the amplitude of the oscillations in each laser is different, as is shown in Fig. 2.11. There lies the localized synchronization concept by which two mutually coupled systems can exhibit synchronized oscillations with different amplitudes. We also note that by increasing further the coupling delay larger ratios between the amplitudes of both lasers can be achieved, as is illustrated in Fig. 2.12.

The correlation degree, defined as the maximum of the cross-correlation function, is relatively high $(0.96 - 1)$ for the entire bifurcation diagram. The correlation degree is almost perfect during the in-phase and anti-phase limit
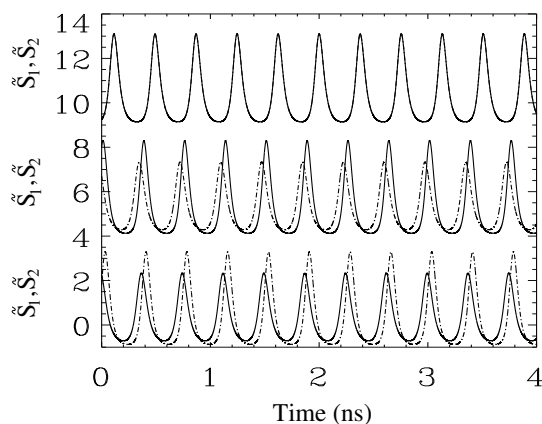
Figure 2.11: Temporal series of the lasers when operating in the SLC and ALC. The time traces has been vertically displaced for clearness reasons. Top: the lasers oscillating with in-phase dynamics on the SLC; middle: the lasers are operating in one of the ALC and pulsating with different amplitudes; and bottom: changing the initial conditions the lasers operate in the other ALC. Solid line: laser 1; dashed line: laser 2.
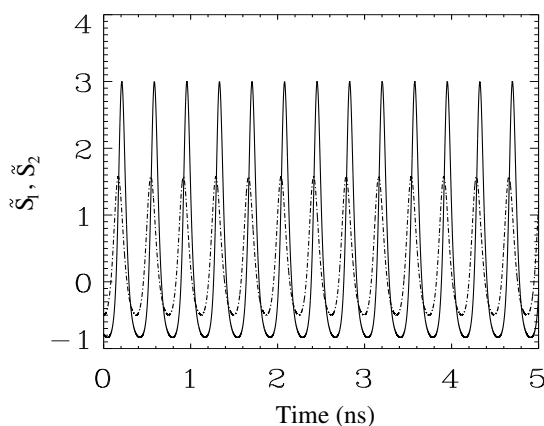
Figure 2.12: Increasing the coupling delay time to $T = 530$ ps, the ratio between amplitudes becomes as large as 2. Solid line: laser 1; dashed line: laser 2.

cycles whereas a small drop in correlation can be observed during the localized synchronization.

Different type of structures and dynamical regimes show up when the bifurcation parameter considered is the coupling strength. Fig. 2.13 shows the bifurcation diagram, maximum of the cross-correlation function, and phase difference between the two laser signals as a function of the coupling rate κ_c. Starting from an uncoupled configuration at the point $\kappa_c = 0$, the phase
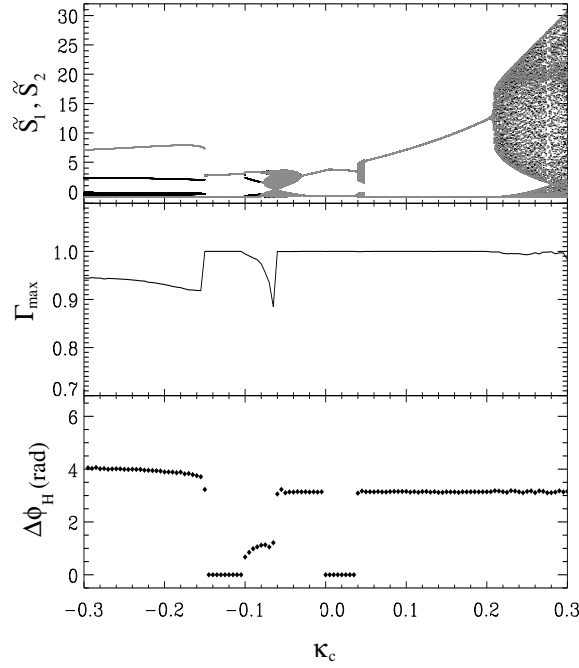
Figure 2.13: From top to bottom: bifurcation diagram for $\tilde{s}_1$ and $\tilde{s}_2$ when changing κ_c, maximum of the cross-correlation function Γ, and mean Hilbert phase difference. The feedback parameters are $\kappa_f = 0.3$ and $\tau = 1$ ns, while the coupling delay time is fixed at $T = 500$ ps.

difference depends on the initial conditions and has been set at zero for convenience. Upon increasing the coupling strength we observe how the two oscillators remain in an in-phase limit cycle. Further increasing the coupling strength leads to a sudden transition to quasi-periodic behavior in both lasers whose phase difference slightly oscillates around π. After this island of quasi-periodic behavior, which appears from $\kappa_c = 0.04$ to $\kappa_c = 0.047$, a regime with anti-phase periodic oscillations is reached. The amplitude of this limit cycle grows with the coupling strength until it reaches the value $\kappa_c = 0.2$. Beyond that value a complex dynamics develops. For slightly negative couplings, $\kappa_c \in (-0.03, 0)$, we obtain an anti-phase dynamics. When decreasing the coupling rate from zero the system enters into a chaotic behavior area which ends with a symmetry-restoring bifurcation around $\kappa_c \sim -0.1$. Before this point is reached the two lasers have passed through a regime of localized synchronization with a phase difference approaching zero as the coupling tends to the symmetry-restoring bifurcation point. In-phase oscillatory behavior is then observed until the coupling value is decreased down to $\kappa_c = -0.15$. Beyond this point and at least until the minimum coupling strength we studied ($\kappa_c = -0.3$) the two lasers oscillate with very different amplitudes, but more important the laser with smaller amplitude enters into a period-two state while the one with larger amplitude remains in a period-one state. This con-

stitutes the second type of asymmetric dynamical regime we have identified for this perfectly symmetric system. We notice that associated to the sudden jump to these asymmetric limit cycles there is a discontinuous change in the amplitude and frequency of the oscillations in both lasers. It is also worth noting that the type of phase dynamics (in-phase or anti-phase) is not univocally determined by the sign of the coupling interaction as it happens with the simple Adler equation describing the phase difference in non-delayed coupled oscillators.

An important point we have already considered is the study of the relative dynamics between the two lasers when they operate as self-sustained oscillators. Regarding this point, we have numerically observed that both in-phase and anti-phase dynamics appear for both positive and negative coupling coefficients at certain values of the coupling delay time T. However, by increasing the feedback strength and the delay time we can force the lasers to operate in a chaotic regime even when they are uncoupled. In contrast to what occurs in the optically coupled face-to-face semiconductor lasers [25], we find that the isochronal (zero-lagged) solution between the two lasers is stable in a wide range of operation. This means that the two lasers are simultaneously exhibiting the same chaotic oscillations even they are spatially separated. This is shown in Fig. 2.14, where the synchronization return plot and the cross-correlation function between the laser intensities are shown. We can see there that the maximum of autocorrelation occurs at zero time shift between the intensity signals, in agreement with the experimental findings [9].
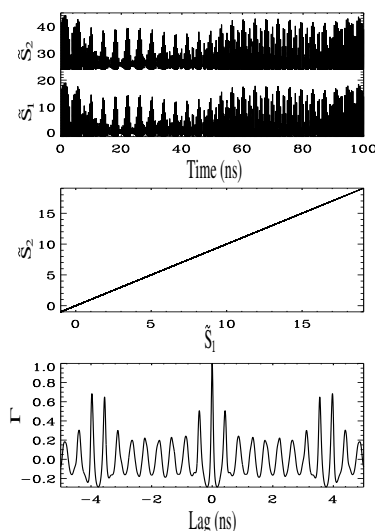
**Figure 2.14**: Top: chaotic temporal series of the lasers intensities after coupling; middle: synchronization plot; bottom: cross-correlation function Γ between the two chaotic outputs. When uncoupled, both lasers operate in the chaotic regime due to their feedbacks loops with $\kappa_f = 0.4$ and $\tau = 3.5$ ns. The coupling strength is $\kappa_c = 0.05$ while the coupling delay is $T = 3.85$ ns.

2.3.2.b Slightly mismatched systems: Arnold Tongues

Another fundamental aspect in coupled dynamical systems is its locking behavior. In particular the frequency locking properties of two coupled oscillators is a subject of wide interest for both theoretical and practical applications. In fact, the phenomenon of adjusting the internal rhythms of a system by an external or mutual perturbation is one of the most investigated effects in the synchronization concept [20]. Here, we are interested in studying the effect of the coupling delay time on these locking properties. In particular, we focus on the dependence of the Arnold tongues size (or frequency locking regions in the coupling strength versus detuning plane) on the coupling delay time between lasers. To this end, we retake the configuration of two isolated lasers that are self-pulsating due to their feedback loops. By changing the delay feedback time in one of the lasers, a detuning between the frequencies of their periodic solutions can be easily induced by hardly changing their amplitudes.

Fig. 2.16 shows the difference of the frequencies of the lasers after couple them as a function of the uncoupled detuning. Each curve in the figure correspond to different delay times in the coupling line. The plateau exhibited by these curves amounts to the width of the Arnold tongues at the coupling strength we are considering. The strong dependence on T is quite evident.
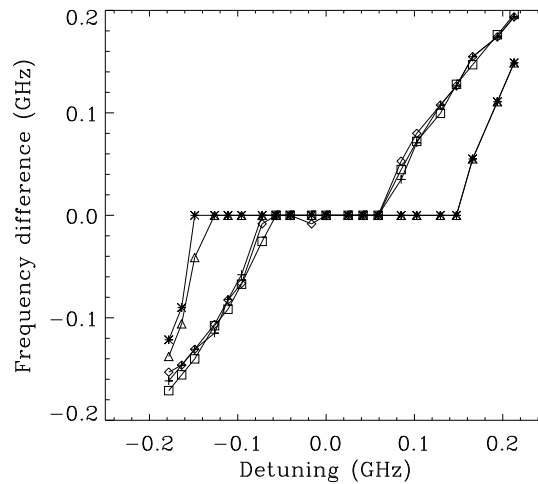
Figure 2.15: Difference of frequencies of the oscillations of the lasers once coupled as a function of the detuning. $T=0$ (squares), $T = 1/4\nu_0$ (crosses), $T = 1/2\nu_0$ (asterisks), $T = 3/4\nu_0$ (diamonds), and $T = 1/\nu_0$ (triangles), where ν_0 is the frequency of oscillations when the lasers are uncoupled at zero detuning. The feedback and coupling strengths are $\kappa_f = 0.3$, and $\kappa_c = 0.1$, respectively. The bias is $\tilde{J} = 1/3$.

Now, varying the coupling strength we numerically compute the width of the former plateaus. This enable us to construct the complete Arnold tongue, which is shown in Fig. 2.16 for different coupling delay times. We recall that

within the Arnold tongue both coupled lasers lock their oscillations into a single frequency. The main result here is the capability of the coupling delay time to modify the width of the Arnold tongues by a factor that can be as large as three. We notice that for any possible application where a good locking state between lasers is required, the effect of the delay time can be quite important on its robustness. Another interesting feature is that a non-zero value of T is able to enlarge the frequency locking zone as compared with the zero-delay-time case. This feature is, for instance, not contemplated in the simple Kuramoto description of two interacting delayed oscillators. In the latter, although the coupling delay time produce multistability, a variation of its value is unable to increase the size of the Arnold tongue with respect to the zero-delay case [26], unless a frustration phase parameter is included.
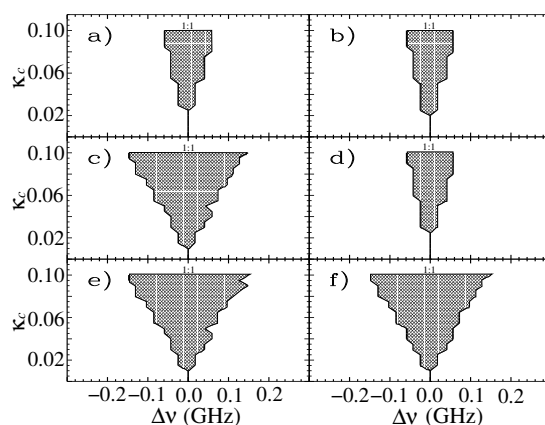
Figure 2.16: 1:1 Arnold tongues for different coupling delay times. a), b), c), d), e), and f) panels correspond to $T = 0$, 1/4, 1/2, 3/4, 1, and 2 times the natural period of the oscillations when the lasers are uncoupled, which is about 348 ps. The feedback strength is $\kappa_f = 0.3$. The bias is $\tilde{J} = 1/3$.

In the next section, we turn into the experimental verification of some of the most relevant behaviors that have been theoretically and numerically predicted in this section, namely, the amplitude quenching or "death by delay" and the isochronous chaotic synchronization.

2.4   Experimental Results

In the experiments, the lasers are InGaAsP/InP single-mode DFB lasers both operating at 1.299 μm wavelength and temperature stabilized at 21 °C. The two lasers, which are chosen from the same wafer, are closely matched in their characteristics to be highly identical. The photodetectors are InGaAs photodetectors with a 6-GHz bandwidth, and the amplifiers are Avantek SSF86 amplifiers with $0.4 - 3$ GHz bandpass characteristics. The laser intensities

measured by the photodetectors are recorded with a Tektronix TDS 694C digitizing real-time sampling oscilloscope with a 3-GHz bandwidth and a digitizing rate up to 1×10^{10} Samples/s. Both the coupling and feedback strengths are easily adjusted by changing the attenuation of the optical power in the coupling and feedback lines, respectively. The coupling and feedback delays are also adjusted by varying the optical path lengths of these lines.

Starting with an experimental scheme similar to that sketched in Fig. 2.2, we are able to experimentally reproduce the "death by delay" effect when varying the coupling delay time as it was first observed in Ref. [9] for semiconductor laser setups. When uncoupled, both lasers exhibit an oscillatory behavior due to their feedback loops. However, as soon as the coupling strength and delay are adjusted to make the system fall into a "death island", an amplitude shrinkage in the oscillations is observed. Fig. 2.17 shows the dynamical states of the two lasers before, inside, and after passing over a "death island", as T is varied from 14.95 ns to 15.45 ns. Due to experimental limitations, no shorter delays were able to be explored, although it is expected that the quenching of the oscillations can be found for shorter delays. Multiple "death island" are found as predicted by the theoretical analysis although they continue to appear for larger delay times than expected from the analysis of the idealized model of Eqs (2.1)-(2.6).

Within the same experimental setup, and just by choosing appropriate strengths and delays in such a manner that both lasers are driven to a chaotic state, we can also study the issue of the chaos synchronization between lasers [9]. Fig. 2.18 shows the synchronization plot and the cross-correlation function between the two laser outputs for coupling delay times of $T_1 = T_2 = 15.4$ ns. It is clear from the figure that both lasers exhibit highly correlated chaotic oscillations. The maximum of the cross-correlation function is located at the zero-lag point and is as high as 0.9. If we allow for different coupling delay times in each one of the coupling lines between lasers (i.e., $T_1 \neq T_2$), then we also observe how the largest peak of the correlation function shifts away from the center by a magnitude of $|(T_2 - T_1)/2|$ and with a direction dependent on which coupling delay time is shorter.

These experimental results agree qualitatively with the results obtained from numerical simulations, and provide the verification that the most interesting features predicted in this system are robust enough to be observed in a real system.
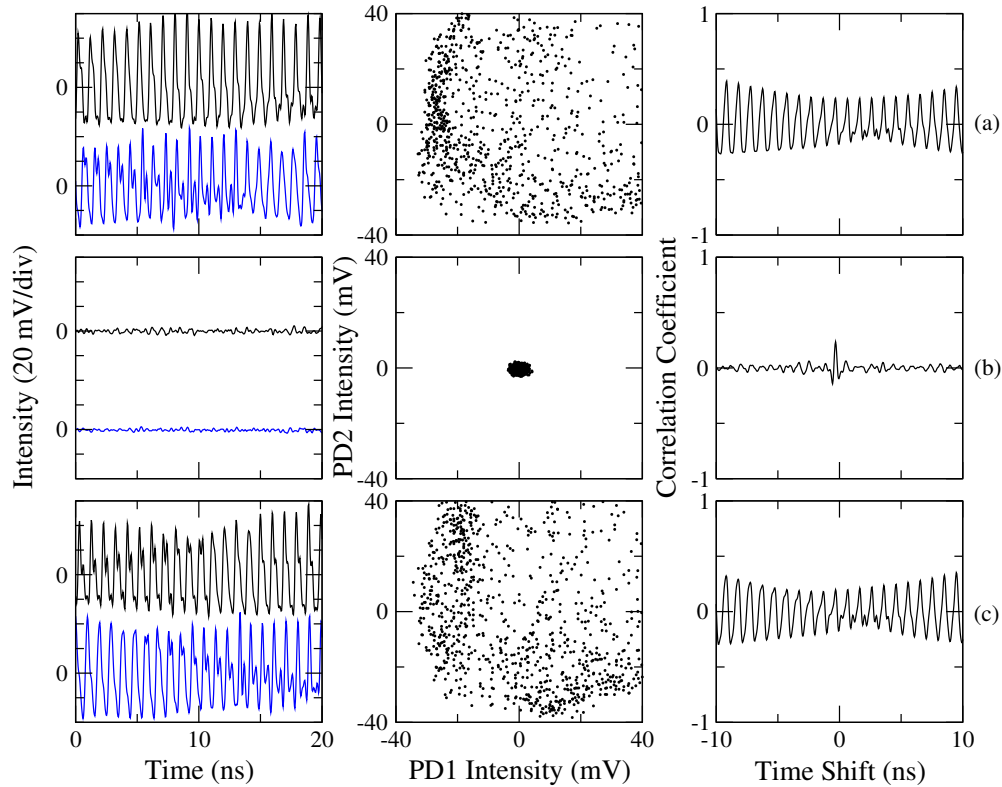
Figure 2.17: From top to bottom, sequence of dynamical states showing the evolution of the laser characteristics before, inside and after passing through a death island, respectively. The coupling delay time T is varied from 14.95 ns to 15.45 ns.
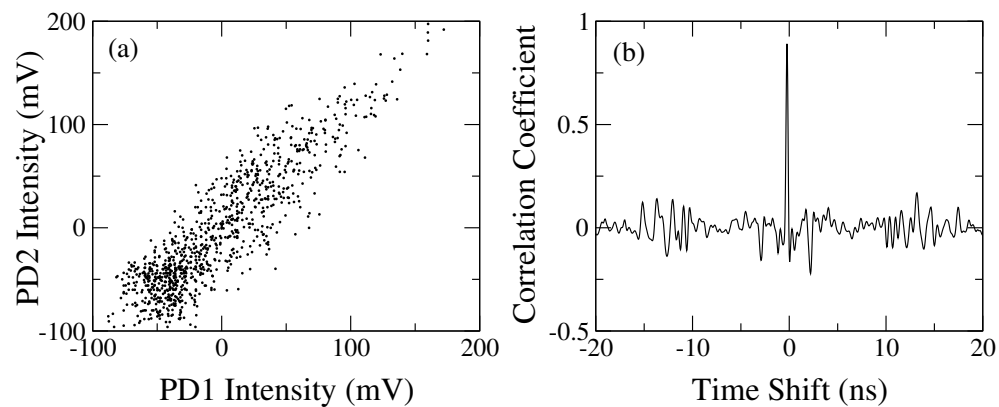
Figure 2.18: Chaos synchronization induced by mutual coupling. Left panel shows a typical synchronization plot between the two laser outputs. Right panel contains the cross-correlation function Γ between the two laser intensities.

Chapter 3

Conclusions

3.1 Conclusions

In summary, we have theoretically investigated the nonlinear dynamics and synchronization properties of two bidirectionally coupled semiconductor lasers subject to optoelectronic feedback loops. We have presented analytical and numerical studies for this system from which we highlight the following points:

- The stability analysis performed provides a first understanding of the mechanisms leading to instability, and the exact role played by the different parameters (coupling and feedback strengths and delay times) in such a process.

- In particular, we have found a new scenario for the quenching of the oscillations that occurs in the absence of delay time in the coupling line and even for identical oscillators. We attribute this interesting behavior to the inclusion of delayed feedback loops, which physically act as an additional memory effect in the system.

- We have concentrated on the synchronization properties of both lasers when they operate as limit cycle oscillators. We have investigated the synchronization scenario that occurs upon increase of the mutual coupling strength and coupling delay time. When varying the coupling delay time, we have identified a sequence for the formation of in-phase, and anti-phase limit cycles separated by symmetry-breaking bifurcations leading to localized synchronization between the lasers. We have also considered the slightly mismatched operation of the lasers. We have seen that a delay time in the coupling between the lasers may improve the capability to lock their oscillations.

- Analytical and numerical predictions are in qualitative agreement with the experimental findings of "death by delay" and synchronization scenario that have been reported in Ref.[9].

- For future work on this setup, it would be interesting to consider several asymmetries in the system such as different delay times and asymmetric coupling strengths between the lasers. Finally, the study of the unfolding of the various codimension-two points and some global phenomena like excitability[27] in our laser setup could be quite interesting.

In a similar configuration we have already started the investigation of the mutual coupling of vectorial oscillators. Taking the so-called spin-flip model we study the synchronization between the polarization of the light emitted by two mutually coupled VCSEL's. Several polarization switchings induced by the coupling or detuning have been numerically observed. Interesting results concerning the polarization diffusion in synchrony between two perfect isotropic VCSEL's are now studied. Moreover, and taking advantage of the polarization bistability that this type of laser exhibits, we have in mind the exploration of the effect of the delay in the mutual interaction between bistable systems. In particular, we are interested in the synchronization properties of the jumps between the potential wells in the two lasers, either induced by noise or modulation of the barrier depth. That is, we want to study the synchronization of jumps in coherence and stochastic resonance systems.

Finally, the extension of some of the synchronization results we have considered here to a larger number of coupled lasers is of great interest. We have also performed some preliminary numerical simulations concerning this issue. They show that the number of units and topology of the network of lasers being coupled is of fundamental importance in the synchronization properties and future work will be with no doubt focused on the investigation of this and related topics.

Bibliography

[1] J. D. Farmer, "Chaotic attractors of an infinite-dimensional system," *Physica D*, vol. 4, p. 366, 1982.

[2] D. V. Ramana Reddy, A. Sen, and G. L. Johnston, "Time delay induced death in coupled limit cycle oscillators," *Phys. Rev. Lett.*, vol. 80, p. 5109, 1998.

[3] S. Strogatz, "Death by delay," *Nature*, vol. 394, p. 316, 1998.

[4] R. Herrero, M. Figueras, J. Rius, F. Pi, and G. Orriols, "Experimental observation of the amplitude death effect in two coupled nonlinear oscillators," *Phys. Rev. Lett.*, vol. 84, p. 5312, 2000.

[5] A. Takamatsu, T. Fujii, and I. Endo, "Time delay effect in a living coupled oscillator system with the plasmodium of physarum polycephalum," *Phys. Rev. Lett.*, vol. 85, p. 2026, 2000.

[6] D. V. Ramana Reddy, A. Sen, and G. L. Johnston, "Experimental evidence of time-delay-induced death in coupled limit-cycle oscillators," *Phys. Rev. Lett.*, vol. 85, p. 3381, 2000.

[7] H. D. I. Abarbanel, N. F. Rulkov, and M. M. Sushchik, "Generalized synchronization of chaos: The auxiliary system approach," *Phys. Rev. E*, vol. 53, p. 4528, 1996.

[8] D. G. Aronson, G. B. Ermentrout, and N. Koppel, "Amplitude response of coupled oscillators," *Physica D*, vol. 41, p. 403, 1990.

[9] S. Tang, R. Vicente, M. Chiang, C. R. Mirasso, and J. M. Liu, "Nonlinear dynamics of semiconductor lasers with mutual optoelectronic coupling," *IEEE J. of Selected Topics in Quantum Electron. (accepted)*, 2004.

[10] S. Tang and J. M. Liu, "Chaotic pulsing and quasi-periodic route to chaos in a semiconductor laser with delayed opto-electronic feedback," *IEEE J. of Quantum Electron.*, vol. 37, p. 329, 2001.

[11] R. Vicente, S. Tang, J. Mulet, C. R. Mirasso, and J. M. Liu, "Dynamics of semiconductor lasers with bidirectional optoelectronic coupling: Stability, route to chaos and entrainment," *Phys. Rev. E (Accepted)*, vol. 70, 2004.

[12] J. Guckenheimer, P. Holmes, and F. John, *Nonlinear Oscillations, Dynamical Systems, and Bifurcations of Vector Fields*. Springer Verlag, 1997.

[13] K. Engelborghs, T. Luzyanina, and G. Samaey, "Dde-biftool v. 2.00 user manual: a matlab package for bifurcation analysis of delay differential equations.," *Technical Report TW-330, Department of Computer Science, K. U. Leuven, Leuven, Belgium*, 2001.

[14] H. Su and J. M. McCarthy, "Classification of designs for rrss linkages," *Proceedings of DETC'01*, p. 1, 2001.

[15] L. Yang, X. R. Hou, and Z. B. Zeng, "A complete discrimination system for polynomial," *Mathematic Mechanization Preprints*, vol. 14, p. 98, 1996.

[16] R. L. Williams II and C. F. Reinholtz, "Mechanism link rotability and limit position analysis using polynomial discriminants," *ASME J. of Mechanisms, Transmissions, and Automation in Design*, vol. 109, p. 178, 1987.

[17] H. Su, C. L. Collins, and J. M. McCarthy, "Classification of rrss linkages," *Mechanism and Machine Theory*, vol. 37, p. 1413, 2002.

[18] J. B. Ermentrout and N. Kopell, "Oscillator death in systems of coupled neural oscillators," *SIAM J. Appl. Math.*, vol. 50, p. 125, 1990.

[19] D. V. Ramana Reddy, A. Sen, and G. L. Johnston, "Time delay effects on coupled limit cycle oscillators at hopf bifurcation," *Physica D*, vol. 129, p. 15, 1999.

[20] A. Pikovsky, M. Rosenblum, and J. Kurths, *Synchronization: A Universal Concept Nonlinear Science*. Cambridge University Press, 2002.

[21] B. F. Kuntsevich and A. N. Pisarchik, "Synchronization effects in a dual-wavelength class-b laser with modulated losses," *Phys. Rev. E*, vol. 64, p. 046221, 2001.

[22] A. Poularikas, *The Transforms and Applications Handbook*. CRC Press and IEEE Press, 1996.

[23] R. Kuske and T. Erneux, "Localized synchronization of two coupled solid states lasers," *Optics Communications*, vol. 139, p. 125, 1997.

[24] A. Hohl, A. Gavrielides, T. Erneux, and V. Kovanis, "Localized synchronization in two coupled nonidentical semiconductor lasers," *Phys. Rev. Lett.*, vol. 78, p. 4745, 1997.

[25] T. Heil, I. Fischer, W. Elsasser, J. Mulet, and C. Mirasso, "Chaos synchronization ans spontaneous symmetry-breaking in symmetrically delay-coupled semiconductor lasers," *Phys. Rev. Lett.*, vol. 86, p. 795, 2001.

[26] H. G. Schuster and P. Wagner, "Mutual entrainment of two limit cycle oscillators with time delayed coupling," *Progress of Theoretical Physics*, vol. 81, p. 939, 1989.

[27] B. Krauskopf, K. R. Schneider, J. Sieber, S. M. Wieczorek, and M. Wolfrum, "Excitability and self-pulsations near homoclinic bifurcation in semiconductor laser systems," *Optics Communications*, vol. 215, p. 367, 2003.

CURRICULUM VITAE

Raúl Vicente Zafra

Personal Data

First name	: Raúl
Surnames	: Vicente Zafra
Date of birth	: 11/23/1979
Place of birth	: Palma de Mallorca, (Spain)
Nationality	: Spanish
Civil Status	: Single
DNI	: 43111438-P
Address	: 100 San Rafael, Palma de Mallorca, Baleares
Post Code	: 07008
Home Phone	: +34 971 246598
Office Phone	: +34 971 172505
e-mail	: raulv@imedea.uib.es
URL	: http://www.imedea.uib.es/~raulv

Academic Degrees

Degree: M.Sc. in Physics
Center: University of the Balearic Islands
Years: 1997/98-2000/01

Current Affiliation

1. Scolarship holder of a Formación del Personal Investigador (FPI) Fellowship of the Ministerio de Educación y Cultura of Spain since 07/01/2002 at the University of the Balearic Islands.

Awarded Fellowships

1. Fellowship of Ayuda al Estudio del Ministerio de Educación y Cultura in the years 1997/98, 1998/99, 1999/00, and 2000/01.

2. Collaboration Fellowship of the Ministerio de Educación y Cultura with the Physics Department of the University of the Balearic Islands during the academic year 2000/01 with the project "Relativistic Star Models".

3. Collaboration Fellowship under the European Community project OC-CULT from 10/01/2001 to 06/30/2002 under the supervision of Dr. Claudio Mirasso.

Other Merits

1. Premio Extraordinario de Licenciatura de Física (First Class Honors), in the year 2000/01.

2. Second position in the local phase (Balearic Islands) of the "VIII Olimpiada Española de Física", February 1997, Palma de Mallorca, Spain.

3. Bronze Medal in the national phase of the "VIII Olimpiada Española de Física", 04/16/1997 to 04/19/1997, Logroño, Spain.

4. Collaborator Student with the Relativity Group of the Physics Department of the University of the Balearic Islands, 2000/01.

5. Student member of the IEEE.

Specialization Courses

Ph.D. courses in the University of the Balearic Islands

- *Mètodes de simulació numérica en física*. R. Toral. UIB, 2002 [3 credits]

- *Sistemes dinàmics*. O. Piro and E. Hernández. UIB, 2003 [3 credits]

- *Dinàmica d'estructures espaciotemporals*. E. Hernández, O. Piro, and M. San Miguel. UIB 2002 [5 credits]

- *Components de sistemes de comunicacions óptiques per fibra*. C.R. Mirasso. UIB 2002 [3 credits]

- *Làsers de semiconductor*. S. Balle. UIB 2002 [3 credits]

- *Punts quantics i nanoestructures bidimensionals*. A. Puente and L. Serra. UIB 2002 [3 credits]

- *Tècniques de supercomputació*. J. Masso. UIB 2003 [3 credits]

- *Models de cooperació basats en agents*. M. San Miguel. UIB 2002 [3 credits]

- *Comunicaciones Caóticas*, 07/02/2001 to 07/06/2001 , Santander. Organized by the Departamento de Física Moderna of the Universidad de Cantabria and the Instituto de Física de Cantabria (IFCA).

- *Tecnologías Fotónicas Emergentes: Cristales Fotónicos*, 07/15/2003 to 07/19/2003, Valencia. Organized by the Universidad de Valencia and the Comité de Optoelectrónica y Óptica Integrada de la Sociedad Española de Física.

- *Delay Equations and Applications*, 09/08/2003 to 09/12/2003, Workshop organized by the University of Bristol, UK.

Stays at foreign research centers

- 03/01/2003 to 05/31/2003 at the Electrical Engineering Department, University of California at Los Angeles (UCLA), Los Angeles, CA (USA), under the supervision of Professor Jia-ming Liu.

- 01/28/2004 to 06/31/2004 at the Electrical Engineering Department, University of California at Los Angeles (UCLA), Los Angeles, CA (USA), under the supervision of Professor Jia-ming Liu.

Seminars

- *"Open- versus Closed- Loop Performance of Synchronized Chaotic External-Cavity Semiconductor Lasers"*, 09/17/2002, Interdisciplinary Physics Department (IMEDEA), Palma de Mallorca, Spain.

- *"Bidirectionally Coupled Semiconductor Lasers"*, 04/01/2003, Department of Electrical Engineering, UCLA, Los Angeles, USA.

- *"Two-Mode Lasers with Added Degrees of Freedom"*, 05/13/2003, Department of Electrical Engineering, UCLA, Los Angeles, USA.

- *"Simple Interpretation of the Dynamics of Two Mutually Coupled Lasers with Detuning"*, 02/09/2004, Department of Electrical Engineering, UCLA, Los Angeles, USA.

- *"Dynamics of Mutually Coupled VCSELs"*, 06/14/2004, Department of Electrical Engineering, UCLA, Los Angeles, USA.

- *"Nonlinear Dynamics of Mutually Coupled Semiconductor Lasers"*, 10/20/2004, Interdisciplinary Physics Department (IMEDEA), Palma de Mallorca, Spain.

Congress presentations

- *Open- versus Closed- Loop Performance of Synchronized Chaotic External-Cavity Semiconductor Lasers*, 09/06/2002, OCCULT Meeting, Athens (Greece). Oral.

- *Dynamical Properties of Two Mutually Coupled Semiconductor Lasers*, 01/30/2003, SPIE 2003, San Jose (USA). Oral.

- *Analysis and Characterization of the Hyperchaos Generated by Semiconductor Lasers Subject to a Delayed Feedback Loop*, 01/30/2003, SPIE 2003, San Jose (USA). Oral.

- *Complexity and Parameter Mismatch in All-Optical Chaos Encryption Schemes*, 02/14/2003, OCCULT Meeting, Pavia (Italy). Oral.

- *Performance Comparison of Different Encoding Schemes in Chaotic Optical Communication Systems*, 06/27/2003, CLEO-Europe/EQEC, Munich (Germany). Oral.

- *Dynamical Properties of Semiconductor Lasers with Optoelectronic Bidirectional Coupling*, 06/25/2003, CLEO-Europe/EQEC, Munich (Germany). Poster.

- *Analysis and Characterization of the Hyperchaos Generated by Semiconductor Lasers Subject to a Delayed Feedback Loop*, 06/25/2003, CLEO-Europe-EQEC, Munich (Germany). Poster.

- *Dynamics of Two Semiconductor Lasers with Bidirectional Optoelectronic Coupling*, 09/16/2003, Workshop on Dynamics of Semiconductor Lasers, Berlin (Germany). Oral.

- *Effect of Parameter Mismatch on the Performance of an All-Optical Chaos Communication Scheme*, 09/19/2003, OCCULT Meeting, Beçanson, (France). Oral.

- *Analysis and Characterization of the Hyperchaos Generated by Semiconductor Lasers Subject to a Delayed Feedback Loop*, 09/23/2003 to 27/09/2003, Dynamic Days, Palma de Mallorca (Spain), Poster.

- *Simple Interpretation of the Dynamics of Two Mutually Coupled Lasers with Detuning*, 01/28/2004, SPIE 2004, San Jose (USA). Oral.

- *Dynamics of Mutually Coupled VCSELs*, 01/28/2004, SPIE 2004, San Jose (USA). Oral.

- *Dynamics of Mutually Coupled Semiconductor Lasers*, 09/27/2004, XX Trobades científiques de la Mediterranea, Mahon (Spain). Poster.

Publications

Articles

- R. Vicente, T. Pérez, and C.R. Mirasso, *"Open- versus Closed- Loop Performance of Synchronized Chaotic External Cavity Semiconductor Lasers"*, IEEE Journal of Quantum Electronics **38**, pp. 1197-1204 (2002).

- J.M. Buldu, R. Vicente, T. Pérez, C.R. Mirasso, M.C. Torrent, and J. García-Ojalvo, *"Periodic Entrainment of Power Dropouts in Mutually Coupled Semiconductor Lasers"*, Applied Physics Letters, **81**, pp. 5105-5107, (2002).

- J.M. Buldú, M.C. Torrent, J. García-Ojalvo, R. Vicente, T. Pérez, and C.R. Mirasso, *"Low Frequency Fluctuations Entrainment is Enhanced by Coupling"*, Fluctuation and Noise Letters, **3**, pp.127-134, (2003).

- C.R. Mirasso, R. Vicente, P. Colet, J. Mulet, and T. Pérez, *"Synchronization Properties of Chaotic Semiconductor Lasers and Applications to Encryption"*, Comptes Rendus de l'Académie de Sciences, Physique, **5**, pp. 613-622, (2004).

- R. Vicente, S. Tang, J. Mulet, C.R. Mirasso, and J.M. Liu, *"Dynamics of Semiconductor Lasers with Bidirectional Optoelectronic Coupling: Stability, Route to Chaos and Entrainment"*, Physical Review E, **70**, pp. 46216, (2004).

- S. Tang, R. Vicente, M. Chiang, C.R. Mirasso, and J.M. Liu, *"Nonlinear Dynamics of Semiconductor Lasers with Mutual Optoelectronic Coupling"*, IEEE Journal of Selected Topics in Quantum Electronics, Accepted, (2004).

- R. Vicente, S. Tang, J. Mulet, C.R. Mirasso, and J.M. Liu, *"Synchronization properties of two self-oscillating semiconductor lasers subject to delayed optoelectronic mutual coupling"*, Submitted, (2004).

- R. Vicente, J. Dauden, P. Colet, and R. Toral, *"Analysis and Characterization of the Hyperchaos Generated by a Semiconductor Laser Subject to a Delayed Feedback Loop"*, Submitted, (2004).

<div align="center">Proceedings</div>

- T. Pérez, R. Vicente, and C.R. Mirasso, *"Dynamical Entrainment of Unidirectionally Coupled Single-Mode Diode Lasers"*, SPIE Proceedings, **4646**, pp. 479-486, (2002).

- R. Vicente, J. Mulet, S. Tang, C.R. Mirasso, and J.M. Liu, *"Dynamical Properties of Two Semiconductor Lasers with Bidirectional Optoelectronic Coupling"*, **4986**, pp. 440-451, (2003).

- R. Vicente, J. Dauden, P. Colet, and R. Toral, *"Analysis and Characterization of the Hyperchaos Generated by a Semiconductor Laser Subject to a Delay Feedback Loop"*, **4986**, pp. 452-462, (2003).

- R. Vicente, J. Mulet, M. Sciamanna, and C.R. Mirasso, *"Simple Interpretation of the Dynamics of Mutually Coupled Semiconductor Lasers with Detuning"*, **5349**, pp. 307-318, (2004).

- S. Tang, M. Chiand, J.M. Liu, R. Vicente, and C.R. Mirasso, *"Experimentally Observed Dynamical Characteristics of Mutually Coupled Semiconductor Lasers With or Without Optoelectronic Feedback"*, **5349**, pp. 319-330, (2004).

- R. Vicente, and C.R. Mirasso, *"Dynamics of Mutually Coupled VCSEL's"*, **5349**, pp. 331-338, (2004).

Computer experience and languages

- Programming: Fortran, IDL, Basic, Mathematica, Matlab, Maple.

- Operative systems: UNIX, Windows, DOS.

- Languages: Spanish (native), Catalan (good), English (good), French (elementary).